

Article

Assessment of Bearing Capacity of Concrete Piles in Alluvial Soils Using Bio and Swarm-Optimized Artificial Neural Network Models

Jitendra Khatti^{1,*} and Denise-Penelope N. Kontoni^{2,3}¹ Department of Civil Engineering, Rajasthan Technical University, Kota 324010, Rajasthan, India² Department of Civil Engineering, School of Engineering, University of the Peloponnese, GR-26334 Patras, Greece³ School of Science and Technology, Hellenic Open University, GR-26335 Patras, Greece* Correspondence: jitendrakhatti197@gmail.com**How To Cite:** Khatti, J.; Kontoni, D.-P.N. Assessment of Bearing Capacity of Concrete Piles in Alluvial Soils Using Bio and Swarm-Optimized Artificial Neural Network Models. *Bulletin of Computational Intelligence* 2025, 1(1), 53–75. <https://doi.org/10.53941/bci.2025.100004>

Received: 12 August 2025

Revised: 30 August 2025

Accepted: 4 September 2025

Published: 10 September 2025

Abstract: This study presents an optimal performance model for predicting the bearing capacity of concrete piles in alluvial soils by comparing Artificial Neural Network (ANN) models optimized with Particle Swarm Optimization (PSO), Harris Hawks Optimization (HHO), Grey Wolf Optimization (GWO), Genetic Algorithm (GA), and Artificial Bee Colony (ABC). A database of 194 data points was collected from the literature and preprocessed. Multicollinearity and cosine amplitude sensitivity analyses were then performed. Of the dataset, 164 data points were used for training and 30 for testing. Performance evaluation showed that the ABC_ANN model achieved over 95% accuracy in both phases. Further validation through Taylor plots, scores (35 for both training and testing), regression error characteristic curves (areas = 0.1982 for training and 0.1078 for testing), generalizability ranking (first), and uncertainty analyses confirmed the superior predictive capability of the ABC_ANN model. Curve-fitting analysis indicated a slight overfitting (1.97) for the ABC_ANN model, followed by the HHO_ANN model. This overfitting was mainly attributed to multicollinearity in features such as soil layer depth, ground elevation, pile tip elevation, and the standard penetration blow count at the pile shaft (a highly sensitive feature, sensitivity = 0.98). Nevertheless, discrete accuracy metrics consistently verified the robustness of the ABC_ANN model in predicting pile bearing capacity. Therefore, this study identifies the ABC ANN model as an optimal tool to support geotechnical engineers and designers in estimating the bearing capacity of concrete piles

Keywords: artificial bee colony; artificial neural network; multicollinearity; generalizability; uncertainty

1. Introduction

The foundation is the essential element of any superstructure, which transfers the load of the superstructure to the strata. Based on the load-bearing capacity of the strata, the foundation is selected and designed to transfer the load to a deep and more stable strata layer [1]. The pile foundations, a type of deep foundation, are designed for strata with lower bearing capacity, typically due to the presence of a high-water table or fine-grained or expansive soils. The primary reason for constructing pile foundations is to ensure stability and prevent settlement by reaching strata with sufficient bearing capacity. To measure the bearing capacity of the pile foundation, the static analysis (e.g., Meyerhof, Vesic's, and Tomlinson method), dynamic formula (e.g., engineering news formula and Hiley formula), pile load test (e.g., static load and dynamic load test), penetration test (e.g., standard penetration test), wave equation analysis, and finite element method (FEM) are utilized [2,3]. These methods are



Copyright: © 2025 by the authors. This is an open access article under the terms and conditions of the Creative Commons Attribution (CC BY) license (<https://creativecommons.org/licenses/by/4.0/>).

Publisher's Note: Scilight stays neutral with regard to jurisdictional claims in published maps and institutional affiliations.

time-consuming and have complex empirical equations to estimate the bearing capacity (P_U). Conversely, several investigators [4–10] derived different regression equations to estimate the P_U of pile foundation. The selection of design and parametric features limits these methods. Therefore, it is hard to achieve the actual bearing capacity (P_U) of the pile foundation.

In recent years, many advanced techniques have been developed to estimate the bearing capacity of foundations, and artificial intelligence (AI) is one of them. The AI techniques are advanced than the empirical equations. These techniques (e.g., machine, deep, and hybrid learning) are highly capable of estimating the bearing capacity of pile foundation. Zhao developed the Naïve Bayes (NB) model and estimated the P_U with a root mean square error (RMSE) of 324.9040 kN [11]. However, the capabilities of the NB model (RMSE = 228.6274 kN and 357.5697 kN using NB_CO and NB_JS0, respectively) were enhanced by implementing the Jellyfish search optimizer (JSO) and the Cheetah optimizer (CO). Umar et al. compared multivariate adaptive regression splines (MARS), Gaussian process regression (GPR), gradient boosting machine (GBM), explainable boosting machine (EBM), and Bayesian additive regression tree (BART) models to find the most accurate model to estimate the P_U [12]. In the published work, it was observed that feature selection plays an important role in each model. Suzuki and Nagai enhanced the P_U estimation using multiple piling data [13]. Sun et al. analyzed the capabilities of the Hunger Game Search (HGS), Tuna Swarm Optimizer (TSO), and salp swarm optimizer (SSA)-based extreme gradient boosting (XGBoost) models [14]. Seo et al. observed that the ram weight and pile diameter are significant features in estimating the P_U of the piles [15]. The investigators reported that the deep neural network (DNN) predicts P_U better than the k-nearest neighbor (kNN) and XGBoost models.

Onyelowe et al. employed soft computing models using standard penetration test blows count (N_t), the number of standard penetration tests (N_n) measured at different depths, the depth of the anticipated elastic settling point (P_e), the depth in meters of the expected phreatic surface (EPTE), the depth of the effective stress point (G_e), the Phreatic surface (PTE) is the depth at which the groundwater table is located, soil exploration depths (i.e., X_1 is the initial, X_2 is the second, and X_3 is the third), and pile diameter (d) of 200 pile tests [16]. The comparison showed that the Kstar model outperformed the M5 tree, elastic net, decision tree, and Correlated Nystrom views (XNV) with an accuracy of 98%. Nhat et al. employed artificial neural network (ANN) model using the dilation angle, friction angle (ϕ), cohesion (c), Poisson's ratio (ν), effective elastic modulus (E), void ratio (e), saturated unit weight (γ_s), unsaturated unit weight (γ_{unsat}), and applied load (P) [17]. Khan et al. utilized more features to estimate the bearing capacity of piles using gene expression programming (GEP). It was concluded that the GEP outperformed the XGBoost, DT, random forest (RF), and support vector machine (SVM) with a mean absolute error of 63.4152kN in the testing phase [18]. Ji optimized the kNN model using Aquila optimizer (AO) and Ebola optimization algorithms (EOS) in predicting the P_U . Several researchers employed conventional (e.g., rock engineering system) and optimized (e.g., reptile search algorithm-RSA, African vulture optimization-AVO, grid search-GS, improved dung beetle optimization-IDBO, improved gray wolf optimizer-IGWO, honey badger algorithm-HBA, coati optimizer-CaO, giant trevally optimizer-GTO, prairie dog optimization-PDO, AO, electric charged particles optimization-ECPO, population-based vortex search algorithm-PVSA, crystal structure algorithm-CSA, fox optimization algorithm-FOX) soft computing approaches (e.g., multilayer perceptron-MLP, kNN, DT, RF, XGBoost, support vector regressor-SVR, kernel-based extreme learning machine-KELM, Gaussian process regression-GPR, kernel ridge regression-KRR, least squares support vector machine-LSSVM, ANN) using the different datasets [19]. The outcomes revealed that the selection of optimization techniques significantly impacts the performance of the soft computing models [20–30]. Arbi et al. optimized the SVM, RF, and XGBoost models using grid search (GS) and random search (RS) algorithms. The performance comparison concluded that the GS_XGBoost model predicted the P_U with a mean absolute error (MAE) of 59.28 kN and an accuracy of 95.2% [31]. Kumar et al. observed that the DNN predicts the pile bearing capacity better than the bidirectional long short-term memory (BiLSTM), conventional long short-term memory (LSTM), recurrent neural network (RNN), and convolutional neural network (CNN) [32]. Khatti et al. compared the 33-hybrid relevance vector machine model to introduce an optimal performance model using effective vertical stress (q_v), plasticity index (PI), undrained shear strength (S_u), time after the end of the drive (T), pile initial capacity (Qf), pile diameter, and length of 126 concrete pile specimens [33]. Many investigators employed AI techniques and observed that the AI models are more accurate than the empirical methods in estimating the bearing capacity of piles. Table 1 summarizes the available models in the literature.

Table 1. Summary of the published models.

S. No.	References	Features: Data	Model	Test RMSE
1	Zhao [11]	$c, \phi, \gamma, \phi', F, A, L$ [231 × 7]	NB_CO	228.6274
2	Umar et al. [12]	A, L, SPT_n, D [125 × 4]	IGPR	278.4500
3	Sun et al. [14]	$v, \phi, E, S_1, L, S_2, S_3, S_4$ [60 × 8]	HGS_XGBoost	169.4300
4	Seo et al. [15]	d, L, D_H (EOID, Restrike), Ram, S (EOID, Restrike), T, D [217 × 9]	DNN	661.1890
5	Seo et al. [15]	d, L, D_H (EOID, Restrike), Ram, S (EOID, Restrike), T, D [217 × 9]	DNN	1142.4000
6	Onyelowe et al. [16]	$d, X_1, X_2, X_3, PTE, Ge, EPTE, Pe, N_n, N_t$ [200 × 10]	kstar	49.3300
7	Ji [19]	$d, X_1, X_2, X_3, PTE, Ge, EPTE, Pe, N_n, N_t$ [200 × 10]	EOS_kNN	39.0000
8	Hu [20]	$c, \phi, \gamma, \phi', F, A, L$ [231 × 7]	RSA_MLP	126.7000
9	Eslami et al. [22]	$N_n, d, WT, D, HD_{max}, HD_{min}, H_{AL}, LT, HN_{1-6}, UH_{SPT}, UH_d, UH_D, LH_{SPT}, LH_d, LH_D$ [110 × 15]	DT	-
10	Chen et al. [23]	L, d, SS_{UD}, τ [65 × 4]	IDBO_KELM	4.7875
11	Cai et al. [24]	$c, \phi, \gamma, \phi', F, A, L$ [231 × 7]	IGWO_GPR	276.1000
12	Yousheng et al. [25]	d, L, CD, ST [150 × 4]	KRR	52.6700
13	Yaychi and Esmacili-Falak [26]	$d, X_1, X_2, X_3, X_p, X_g, X_t, X_m, N_s, N_t$ [472 × 10]	CaO_RF	38.3122
14	Yang et al. [27]	$c, \phi, \gamma, \phi', F, A, L$ [231 × 7]	PDO_LSSVM	213.7700
15	Xu and Zhu [28]	$d, X_1, X_2, X_3, PTE, Ge, EPTE, Pe, N_n, N_t$ [200 × 10]	ECPO_SVR	35.6510
16	Shen [30]	$d, X_1, X_2, X_3, PTE, Ge, EPTE, Pe, N_n, N_t$ [200 × 10]	CSA_ANN	24.8840
17	Arbi et al. [31]	$d, X_1, X_2, X_3, X_p, X_g, X_t, X_m, N_s, N_t$ [472 × 10]	GS_XGBoost	59.2800
18	Kumar et al. [32]	d, L, PS, Ram, DH [257 × 5]	DNN	0.0820 *
19	Khatti et al. [33]	$d, L, q_v, PI, Su, T, Q_f$ [126 × 7]	GA_GRVM	146.3962
20	Karakaş et al. [34]	L, A, q_{cend}, q_{cave} [219 × 4]	CatBoost	R = 0.8944
21	Karakaş et al. [34]	L, d, IFR, S, q_{cave} [60 × 5]	XGBoost	R = 0.9327
22	Gu et al. [35]	$d, X_1, X_2, X_3, X_p, X_g, X_t, X_m, N_s, N_t$ [472 × 10]	ANFIS	38.6543
23	Gang [36]	$d, X_1, X_2, X_3, PTE, Ge, EPTE, Pe, N_n, N_t$ [200 × 10]	LHHO_ANFIS	47.5370

Note— c is the cohesion, ϕ is the friction angle, γ is the specific weight of soil, ϕ' is the pile-soil friction angle, F is the flap number, A is the pile area, L is the pile length, SPT_n is the uncorrected number of blows at pile tip, D is the embedded depth, IGPR is the improved GPR, v is the Poisson’s ratio, E is the elastic modulus, S_1 is the earth-filled, S_2 is the silty clay, S_3 is the fully weathered rhyolite, S_4 is the strong weathered rhyolite, D_H is the drop height, S is the sets of EOID and restrike piles, T is the thickness, d is the diameter, EOS_kNN is the Ebola optimized-kNN model, WT is the water table ratio, HD_{min} is the minimum helix diameter, HD_{max} is the maximum helix diameter, H_{AL} is the helix area length, LT is the load type, HN_{1-6} is the helix number 1 to 6, UH_{SPT} is the upper helix SPT, UH_d upper helix diameter, UH_D is the upper helix, LH_{SPT} is the lower helix SPT, LH_d is the lower helix diameter, LH_D is the lower helix depth, SS_{UD} is the undrained shear strength, τ is the average effective vertical stress, CD is the corrosion depth, ST is the spalling thickness, X_p is the top elevation of pile, X_g is the natural ground elevation, X_t is the extra segment pile top’s elevation, X_m is the pile tip’s depth, N_s is the mean SPT blow count along the pile shaft, PS is the pile set, * represents to the normalized results, GA_GRVM is the genetic algorithm-optimized Gaussian kernel-based RVM model, q_{cend} is cone resistance from CPT at the pile tip, q_{cave} is the cone resistance along the pile length, IFR is the incremental filling ratio, S is the setup days, R is performance, ANFIS is the adaptive neuro-fuzzy inference system, LHHO_ANFIS is the leader-harris hawks optimized-ANFIS model.

The literature revealed that the researchers employed conventional and optimized DT, RF, GPR, SVM, SVR, ANFIS, XGBoost, RVM, and kNN models to estimate the bearing capacity of the pile. A few studies have employed conventional and optimized ANN models. Moreover, it has been observed that no investigators have compared bio and swarm-optimized ANN models in estimating the P_U . The soft computing approaches are black-box and may be affected by feature multicollinearity in predicting the P_U . No investigator analyzed the feature multicollinearity and its impact on the performance and overfitting of the models in predicting the P_U . Considering the following gaps in the literature, the novelty of the present investigation is as follows:

- This investigation employs the Particle Swarm Optimization (PSO), Harris Hawks Optimization (HHO), Grey Wolf Optimization (GWO), Genetic Algorithm (GA), and Artificial Bee Colony (ABC)-optimized ANN models and analyzes their capabilities in predicting the bearing capacity of the reinforced concrete piles.
- This work determines the feature multicollinearity of $N_t, N_s, X_m, X_t, X_g, X_p, X_3, X_2,$ and X_1 using variance inflation factor (VIF) method and illustrates the impact of feature multicollinearity on the performance and overfitting of the PSO_ANN, HHO_ANN, GWO_ANN, GA_ANN, and ABC_ANN models in estimating the bearing capacity of the reinforced concrete piles.

This study introduces an optimal performance model, which will help geotechnical engineers and designers determine the bearing capacity of concrete piles without performing field experiments. The $N_t, N_s, X_m, X_t, X_g, X_p, X_3, X_2,$ and X_1 parameters will be used to predict the P_U of concrete piles. To achieve that, a database of 200

reinforced concrete piles has been compiled from the published research by Amjad et al. [37]. The database consists of bearing capacity of pile (P_U), SPT blow count at pile tip (N_t), SPT blow count at pile shaft (N_s), pile tip elevation (X_m), extra pile top elevation (X_t), ground elevation (X_g), pile top elevation (X_p), depth of the third layer of soil embedded (X_3), depth of the second layer of soil embedded (X_2), and depth of the first layer of soil embedded (X_1) of 200 reinforced concrete piles. From the preprocessing (removing outliers and missing values), 194 datasets have been accumulated. The preprocessed database has been analyzed by performing descriptive statistics, frequency distribution, distance correlation, multicollinearity, and sensitivity analyses. Finally, the training and testing databases have been created by randomly selecting 85% and 15% of the 194 datasets.

The ABC_ANN, GA_ANN, GWO_ANN, HHO_ANN, and PSO_ANN models have been trained and tested on 164 and 30 datasets, respectively. The root mean square error (RMSE), mean absolute error (MAE), mean absolute percentage error (MAPE), Nash-Sutcliffe Efficiency Coefficient (NSE), variance accounted for (VAF), performance (R), and Explained Variance Score (EVS) metrics have been measured and analyzed to evaluate the capabilities of each model. In addition, the Taylor plot, score analysis, regression error characteristics (REC) curve, generalizability, and uncertainty analyses have been performed to obtain the optimal performance models. In predicting the bearing capacity of the reinforced concrete piles, the discrete accuracy of each model has been analyzed by a-index (a_{10} , a_{20} , and a_{30}) and prediction of change in direction (PCD). In addition, the curve fitting has been analyzed for each model to understand the behavior of the model on unseen datasets. Finally, an optimal performance model has been obtained and compared with the available models to demonstrate the robustness of the model. Figure 1 presents the flow of the present investigation.

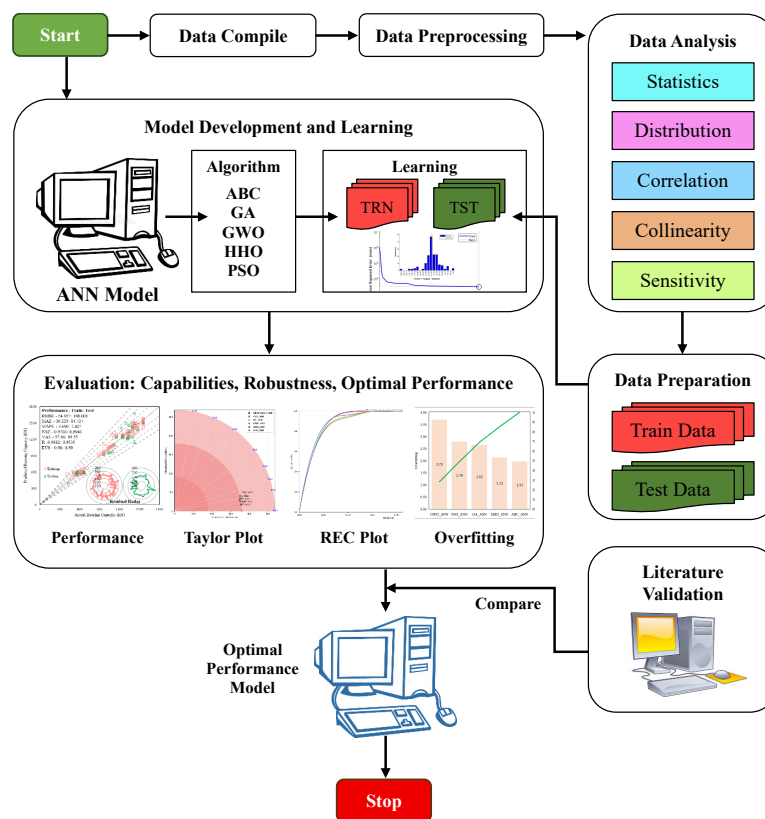


Figure 1. Illustration of the methodology of the present study.

2. Development of Computational Models

2.1. Artificial Neural Networks (ANNs)

Artificial Neural Networks (ANNs) are powerful machine learning models designed to mimic the structure and functioning of the human brain. They consist of interconnected layers of nodes, or “neurons”, that process information by applying weighted connections. Through this mechanism, ANNs learn to transform input data into meaningful outputs, making them highly effective for complex pattern recognition and prediction tasks. ANNs are used for regression, classification, pattern recognition, and forecasting because they are very good at modeling complicated, nonlinear connections in data. The selection of activation functions, learning rate, training technique, and number of hidden layers is an essential determinant of ANN performance. Accurate and reliable results depend

on careful model architecture design and proper normalization of input data. In a range of real-world applications, ANNs offer high predicted accuracy and good generalization with enough training data and an exemplary architecture. This investigation employs a feedforward-backpropagation algorithm-based multilayer perceptron neural network to estimate the bearing capacity of concrete piles. To achieve an excellent prediction, the ANN approach has been optimized by the Bio and Swarm algorithms. These ANN models have been employed and analyzed using the MATLAB R2020a framework.

2.2. Optimization Algorithms

This study optimizes the artificial neural network model by implementing Particle Swarm Optimization (PSO), Harris Hawks Optimization (HHO), Grey Wolf Optimization (GWO), Genetic Algorithm (GA), and Artificial Bee Colony (ABC) algorithms. The reasons for selecting these optimization algorithms have been summarized in Table 2. In addition, a brief discussion has been mapped for each algorithm in the following subsections.

Table 2. Reasons for selecting the optimization algorithms.

Algorithms	Hyperparameter Sensitivity	Advantages	Remarks
ABC	Moderate sensitivity to population size and limit value for abandoning solutions.	<ul style="list-style-type: none"> • Good exploration capability. • Simple and easy to implement. 	<ul style="list-style-type: none"> • May converge slowly due to random scout behavior. • The balance between exploration and exploitation needs tuning.
GA	Highly sensitive to population size, crossover and mutation rates, and selection strategy.	<ul style="list-style-type: none"> • Strong global search. • Handles discrete and continuous problems well 	<ul style="list-style-type: none"> • Requires careful tuning of crossover and mutation rates. • Convergence can be slow if parameters are not well chosen.
GWO	Low to moderate sensitivity to population size and bounds (lb/ub).	<ul style="list-style-type: none"> • Few parameters to tune. • Effective balance of exploration and exploitation 	<ul style="list-style-type: none"> • Simple structure • Struggles with local optima in complex landscapes.
HHO	Moderate sensitivity to population size and escape energy parameter.	<ul style="list-style-type: none"> • Dynamic transition between exploration & exploitation. • Strong local search 	<ul style="list-style-type: none"> • Convergence behavior can vary based on the problem. • Newer and less studied.
PSO	Highly sensitive to inertia weight, cognitive/social factors, and swarm size.	<ul style="list-style-type: none"> • Fast convergence. • Efficient in continuous optimization problems 	<ul style="list-style-type: none"> • Prone to premature convergence. • Performance depends heavily on parameter tuning.

2.1.1. ABC Algorithm

The Artificial Bee Colony (ABC) algorithm is a nature-inspired optimization technique that simulates the foraging behavior of honeybee swarms. Karaboga first presented it in 2005 as a solution to challenging numerical optimization issues [38]. Each member of the colony, employed bees, observer bees, and scout bees, contributes to the exploration and exploitation of the search space in the ABC algorithm. Employed bees explore for food sources, or solutions, and impart this knowledge to bystander bees, who then use probability to select superior solutions. In the absence of existing sources, scout bees randomly investigate new locations. Because the method successfully strikes a balance between exploration and exploitation, it may be used for a variety of optimization problems.

2.1.2. GA Algorithm

The GA is a potent evolutionary optimization method that draws inspiration from genetics and natural selection. It starts with a population of chromosomes, which are potential solutions. GA finds optimum or almost ideal solutions by evolving the population over generations through processes including crossover, mutation, and selection. While crossing and mutation provide diversity, selection rewards those who are more fit. By striking a balance between exploration and exploitation, GA is able to stay clear of local optima. Because of its resilience and versatility, GA is extensively utilized in many domains, including machine learning, engineering, and economics.

2.1.3. GWO Algorithm

The GWO is an optimization algorithm inspired by nature that imitates the hunting habits and social structure of grey wolves. GWO, which was first presented by Mirjalili et al. [39] in 2014, guides the search process by simulating the leadership structures of alpha, beta, delta, and omega wolves. While beta and delta aid in directing the movement of other wolves, the alpha wolf is the ideal answer. Based on the best answers discovered thus far, wolves encircle their prey and adjust their postures. GWO is able to successfully strike a balance between exploration and exploitation due to this encircling and attacking mechanism. Because of its effectiveness and simplicity, GWO is frequently utilized to solve challenging machine learning and engineering problems.

2.1.4. HHO Algorithm

The HHO is a population-based optimization technique that draws inspiration from Harris hawks’ cooperative hunting style. HHO is the best option as it imitates hawks’ sudden pounce attack on prey, as suggested by Heidari et al. [40] in 2019. In response to the prey’s energy, the program dynamically alternates between exploration and exploitation. Hawks scan the landscape extensively during exploration and then narrow their search using a variety of attacking techniques during exploitation. Through this adaptive process, HHO is able to converge and escape local optima effectively. HHO has proven to be highly effective in a variety of scientific and engineering optimization challenges.

2.1.5. PSO Algorithm

The social behavior of fish schools and flocks of birds served as the inspiration for the population-based optimization technique known as PSO. PSO, which was first presented by Kennedy and Eberhart [41] in 1995, finds the best answer by moving a swarm of particles around the search area. Based on both its own and its neighbors’ experiences, each particle modifies its location. Both the particle’s (personal best) and the swarm’s (global best) optimal positions have an impact on the movement. PSO is able to balance exploration and exploitation thanks to this collaboration and information exchange. PSO’s simplicity, efficiency, and speed make it a popular choice for resolving challenging optimization issues.

2.3. Hyperparameter Tuning

The optimized ANN models were fine-tuned using different metaheuristic algorithms, each with specific hyperparameter configurations. For ABC_ANN, the model used the trainlm backpropagation algorithm with 10 hidden layers, a learning rate of 1×10^{-3} , and achieved a convergence curve value of 2.2586×10^3 after 100 iterations using a population size $n = 30$. GA_ANN utilized genetic operations like scattered crossover, Gaussian mutation, and stochastic uniform selection with a population size of 50 and an elite count set to 5% of the population. GWO_ANN applied the Grey Wolf Optimizer with a bounded search space [1,0] to [100,1], achieving a convergence curve of [12.2866,0.0460]. HHO_ANN followed a similar bounding strategy and ran 100 iterations with $n = 30$, yielding a convergence of 2.1282×10^3 . PSO_ANN incorporated a swarm size of 50, inertia weights ranging from 0.1 to 1.1, and a self/social adjustment weight of 1.49. All models used the trainlm learning algorithm and 10 hidden neurons for consistency. Parallel computation was enabled in GA_ANN and PSO_ANN to enhance computational efficiency. The optimal parameter sets differed among the models, reflecting the distinct ways in which each algorithm explores and exploits the solution space. These configurations reflect tailored optimization strategies for enhancing ANN performance across different algorithmic paradigms. Table 3 presents a summary of the hyperparameter configuration of each model. In addition, Figure 2 demonstrates the convergence plot with error histogram of each model in the training phase.

Table 3. Summary of hyperparameter configuration of models.

Models	Configurations
ABC_ANN	Backpropagation algorithm = trainlm, hidden layers = 10, convergence curve = 2.2586×10^3 , learning rate = 1.0×10^{-3} , iterations = 100, $n = 30$, optimal parameters = [28.0397, 0.5592].
GA_ANN	Backpropagation algorithm = trainlm, hidden layers = 10, learning rate = 1.0×10^{-3} , elite count = 0.05*population size, nonlinear constraint algorithm = auglag, crossover fraction = 0.80, crossover function = @crossoverscattered, iterations = 100, population size = 50, population type = double vector, selection function = @selectionstochunif, fitness limit = -inf, mutation function = [Gaussian, 1, 1], use parallel = 1, optimal parameters = [7.4560, 0.1955].
GWO_ANN	Backpropagation algorithm = trainlm, hidden layers = 10, learning rate = 1.0×10^{-3} , lb = [1, 0], iterations = 100, optimal parameters = 2.1750×10^3 , convergence curve = [12.2866, 0.0460], ub = [100, 1].
HHO_ANN	Backpropagation algorithm = trainlm, hidden layers = 10, learning rate = 1.0×10^{-3} , convergence curve = 2.1282×10^3 , lb = [1,0], iterations = 100, $n = 30$, ub = [100,1].
PSO_ANN	Backpropagation algorithm = trainlm, hidden layers = 10, learning rate = 1.0×10^{-3} , optimal parameters = [4.3906, 3.1634], creation function = @pswcreationuniform, Inertia range = [0.100, 1.100], initial swarm span = 2000, iterations = 100, min neighbors’ fraction = 0.25, self and social-adjustment weight = 1.49, swarm = 50, use parallel = 1.

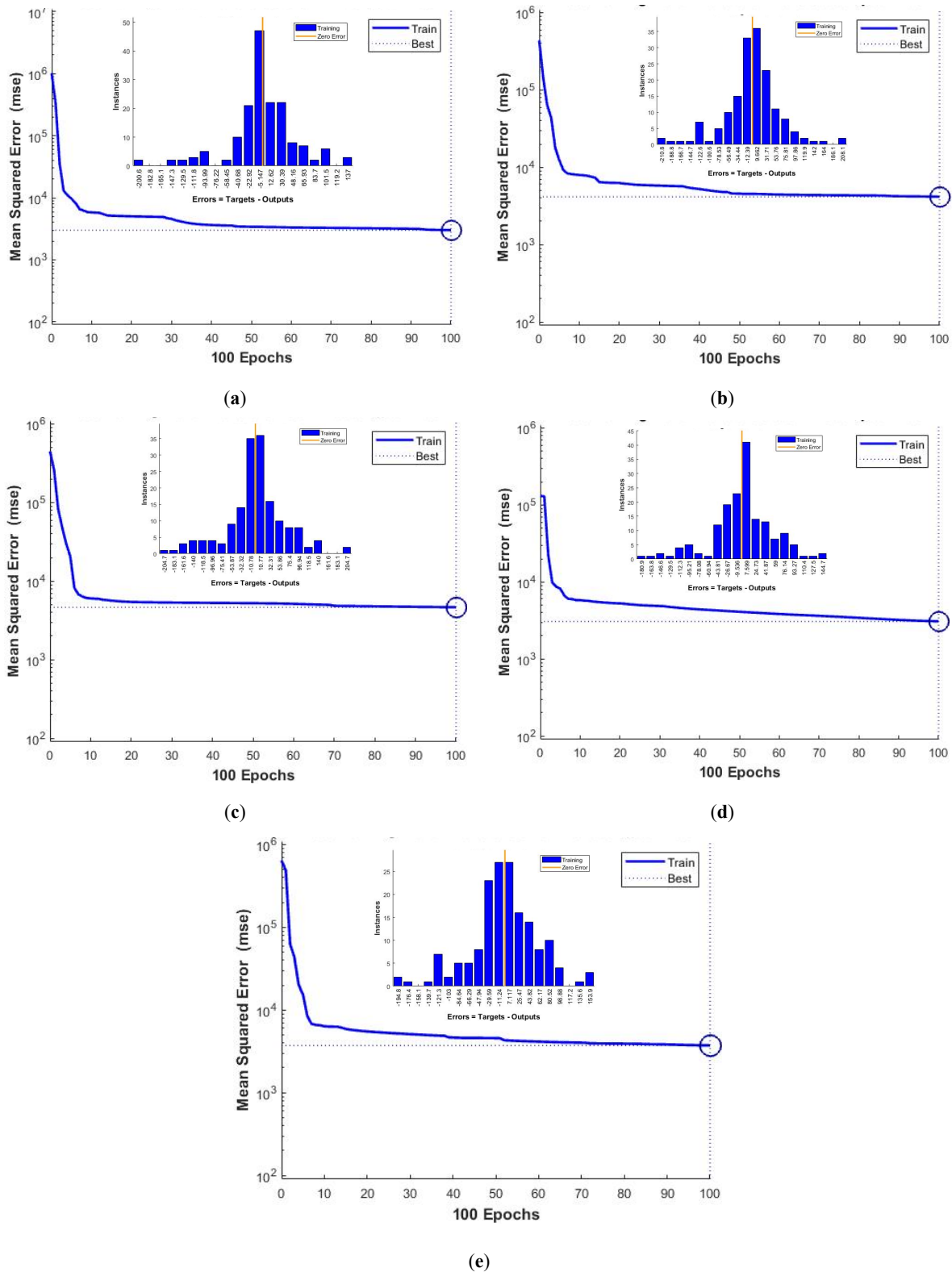


Figure 2. Illustration of convergence plot with error histogram for the (a) ABC_ANN; (b) GA_ANN; (c) GWO_ANN; (d) HHO_ANN; and (e) PSO_ANN models.

3. Data Analysis and Preparation

The present work uses the bearing capacity of 200 reinforced concrete piles, tested at Ha Nam province, Vietnam, as published by Amjad et al. [37]. For testing, a hydraulic jack was placed on the pre-cast squared piles with a closed tip to press the pile at a constant rate of penetration. Finally, a database has been compiled using soil attributes, pile material, and geometry. The database consists of bearing capacity of pile (P_U), SPT blow count at pile tip (N_t), SPT blow count at pile shaft (N_s), pile tip elevation (X_m), extra pile top elevation (X_t), ground elevation

(X_g), pile top elevation (X_p), depth of the third layer of soil embedded (X_3), depth of the second layer of soil embedded (X_2), and depth of the first layer of soil embedded (X_1) of 200 reinforced concrete piles. For quality assurance, the complete database has been preprocessed by performing Z-score analysis to detect outliers and remove missing values. Figure 3 presents the comparison of the database before and after preprocessing. Thus, 194 datasets have been collected from preprocessing.

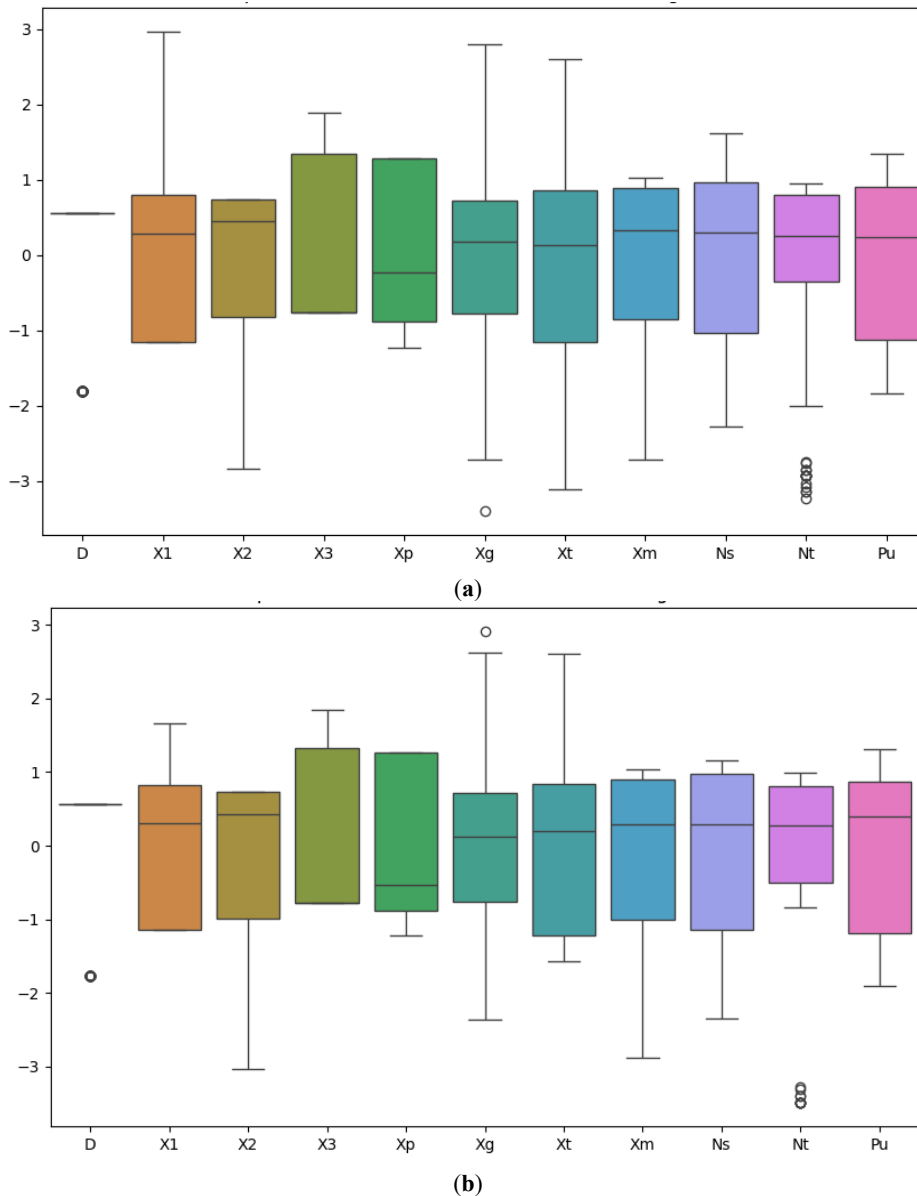


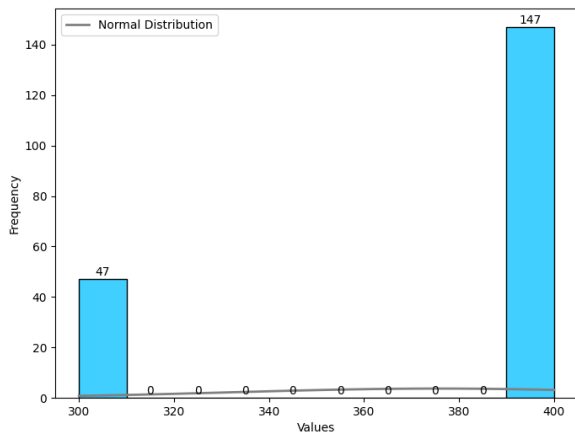
Figure 3. Illustration of the database (a) before and (b) after preprocessing.

To analyze the 194 datasets, the descriptive statistics have been drawn as summarized in Table 4. The D shows a high mean of 375.77 mm with zero interquartile range, indicating identical 25th and 75th percentiles, possibly due to repeated maximum values. Most features like X_1 , X_p , and X_t exhibit low to moderate variability, whereas features such as X_m and X_2 show wider spreads with interquartile ranges of 3.30 m and 2.75 m, respectively. Negative skewness dominates across features such as D, X_2 , X_m , and N_t , indicating a left-tailed distribution, while positive skew is seen in X_3 and X_p . Notably, N_t has high kurtosis (4.41), suggesting a more peaked distribution, while several others, including X_t and P_u , exhibit platykurtic (flattened) behavior. The target variable P_u has a wide range (407.20 kN to 1551.00 kN) and a large standard deviation (355.85 kN), suggesting high variability. Overall, these metrics reflect a dataset with diverse feature distributions, both symmetric and skewed, with varying degrees of spread and peakedness. Figure 4 presents the frequency distribution of features and labels of 194 piles.

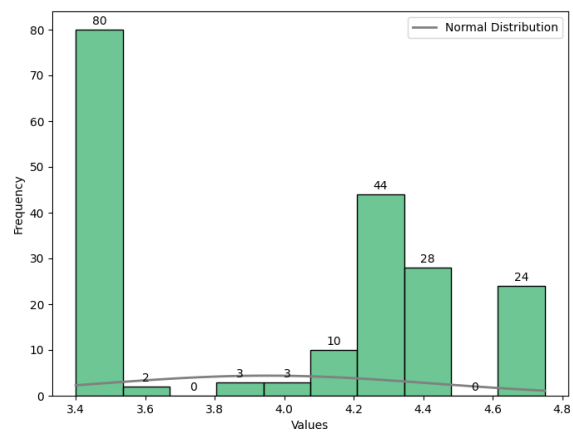
Table 4. Summary of statistics of 194 datasets.

Variables	Unit	Category	Mean	Min	Max	SDev	Skewness	Kurtosis	Q1	Q2	Q3
D	mm	Feature	375.77	300.00	400.00	42.96	-1.20	-0.55	400.00	400.00	0.00
X ₁	m	Feature	3.95	3.40	4.75	0.48	0.00	-1.58	3.40	4.35	0.95
X ₂	m	Feature	6.83	2.00	8.00	1.60	-1.45	1.57	5.26	8.00	2.75
X ₃	m	Feature	0.35	0.00	1.18	0.45	0.70	-1.38	0.00	0.95	0.95
X _p	m	Feature	2.66	1.95	3.40	0.58	0.26	-1.74	2.15	3.40	1.25
X _g	m	Feature	3.52	3.36	3.72	0.07	0.06	-0.35	3.47	3.57	0.10
X _t	m	Feature	2.92	2.00	4.45	0.59	-0.18	-1.10	2.21	3.41	1.20
X _m	m	Feature	13.79	8.80	15.58	1.74	-1.18	0.90	12.06	15.35	3.30
N _s	-	Feature	11.13	6.10	13.63	2.15	-0.68	-0.72	8.68	13.21	4.54
N _t	-	Feature	7.08	4.80	7.73	0.66	-1.90	4.41	6.75	7.61	0.86
P _U	kN	Label	1082.99	407.20	1551.00	355.85	-0.38	-1.34	661.60	1392.00	730.40

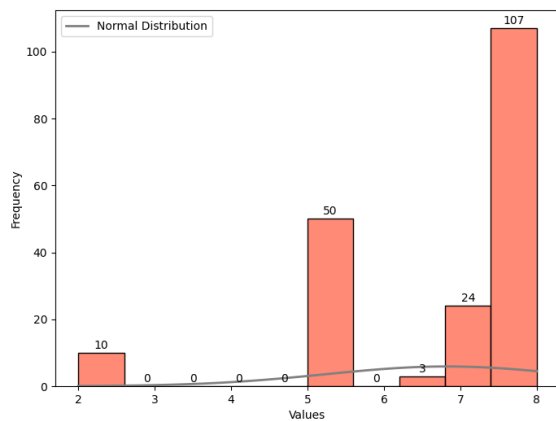
Note: SDev is the standard deviation, Q1 is the first quartile range, Q2 is the second quartile range, and Q3 is the third quartile range.



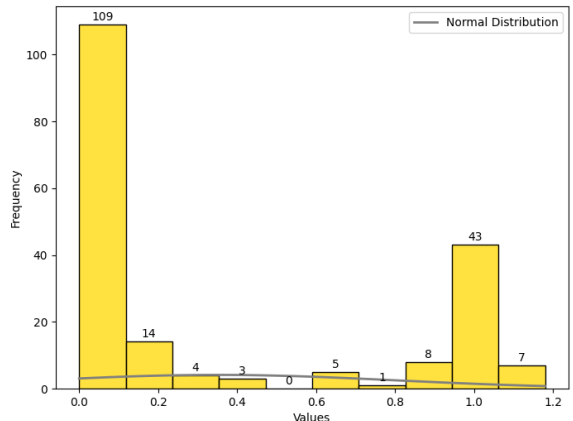
(a)



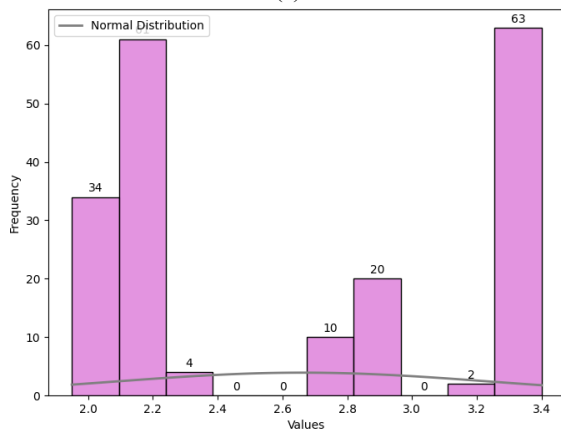
(b)



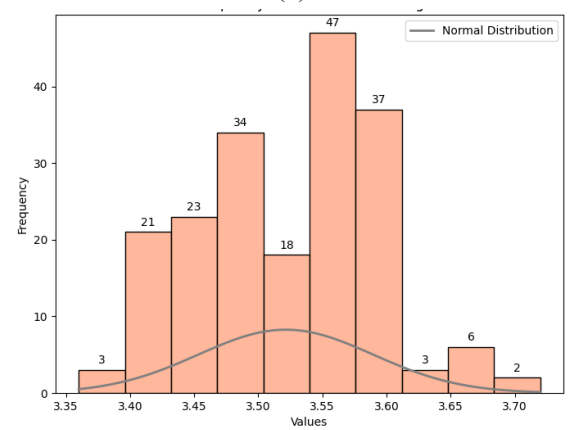
(c)



(d)



(e)



(f)

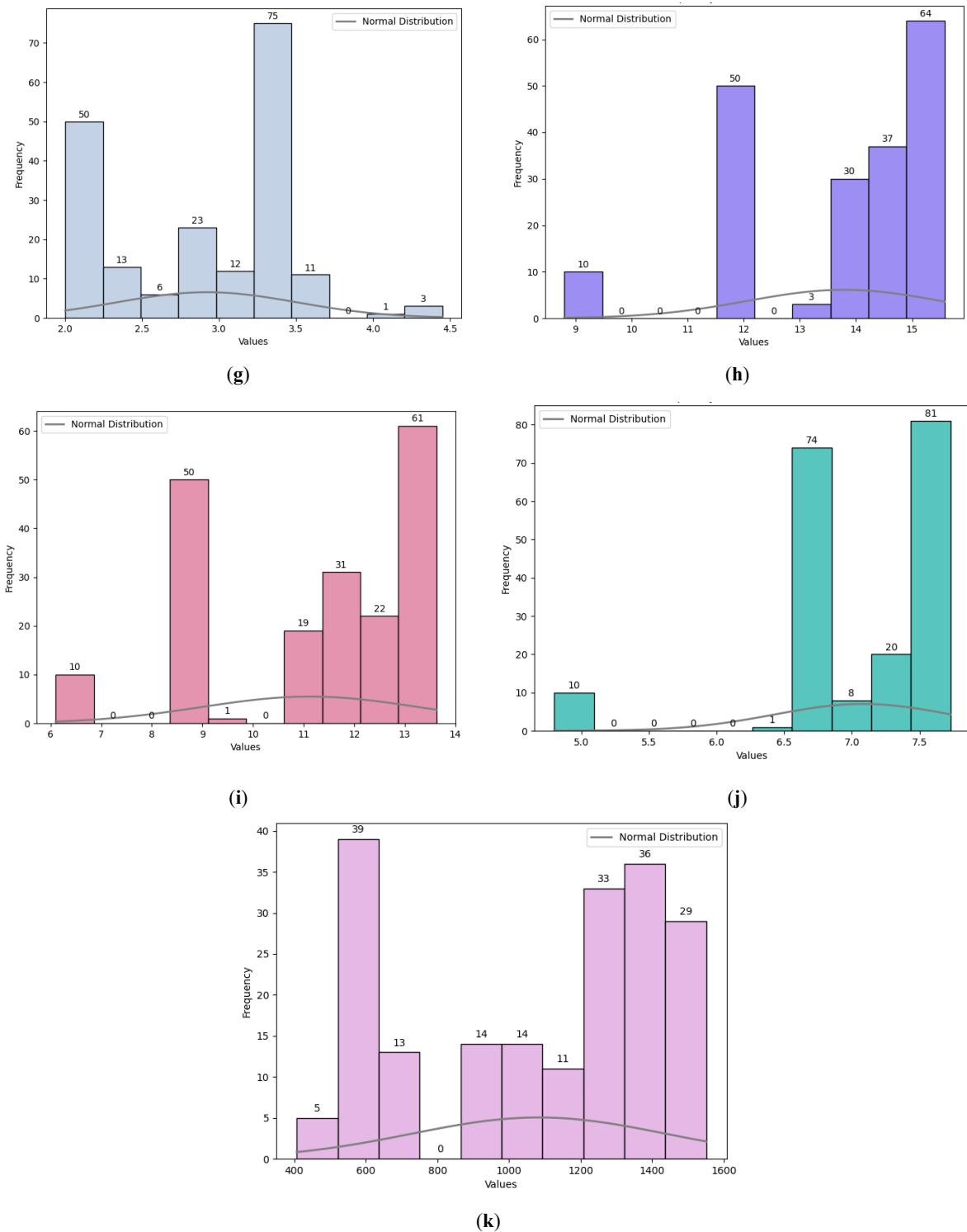


Figure 4. Illustration of frequency distribution of (a) D; (b) X₁; (c) X₂; (d) X₃; (e) X_p; (f) X_g; (g) X_i; (h) X_m; (i) N_s; (j) N_i; and (k) P_U of 194 piles.

Based on the descriptive statistics and frequency distribution plots, it has been decided to map the relationship between variables using the distance correlation coefficient method. This correlation is calculated by dividing their distance covariance by the product of their distance standard deviations [42]. The mathematical formulation of distance correlation is as follows:

$$dCor^2(X, Y) = \frac{dCov^2(X, Y)}{\sqrt{dVar^2(X)dVar^2(Y)}} \tag{1}$$

where *Cov* is the standard Pearson correlation, and *Var* is the variance. The correlation value varies from 0 to 1. The distance correlation (DC) presents no (DC = 0), weak (0 < DC ≤ 0.2), good (0.2 < DC ≤ 0.4), moderate (0.4

< DC ≤ 0.6), strong (0.6 < DC ≤ 0.8), and very strong (0.8 < DC ≤ 1.0) relationships between a pair of data points [43,44]. Figure 5 presents the relationship between the variables of 194 piles using the DC matrix. It can be noted that (a) D very strongly correlates with P_U (=0.803); (b) D has strong relationship with N_s (=0.779), X_m (=0.779), X_p (=0.722), X₂ (=0.794), and X₁ (=0.668); (c) D moderately correlates with X₃ (=0.446), X_g (=0.521), X_t (=0.552), and N_t (=0.584); (d) X₁ very strongly correlates with X_p (=0.964); (e) X₁ has strong relationship with X₂ (=0.605), X₃ (=0.624), X_t (=0.665), X_m (=0.652), N_s (=0.761), and P_U (=0.753); (f) X₂ has very strong relationship with P_U (=0.856), N_t (=0.871), N_s (=0.961), and X_m (=0.986); (g) X₂ strongly correlates with X₃ (=0.657), X_p (=0.723), and X_t (=0.632); (h) X₃ very strongly correlates with N_t (=0.814) and X_t (=0.912); (i) X₃ has strong relationship with N_s (=0.789), X_m (=0.780), and X_p (=0.681); (j) X_p very strongly correlates with P_U (=0.807) and N_s (=0.859); (k) X_p also strongly correlates with X_m (=0.757) and X_t (=0.706); (l) X_g has moderate relationship with P_U (=0.464), N_s (=0.450), and X_m (=0.435); (m) X_t strongly correlates with X_m (=0.729), N_s (=0.736), and N_t (=0.760); (n) X_m very strongly correlates with N_s (=0.981), N_t (=0.896), and P_U (=0.850); and (o) N_s also very strongly correlates with N_t (=0.824) and P_U (=0.886).

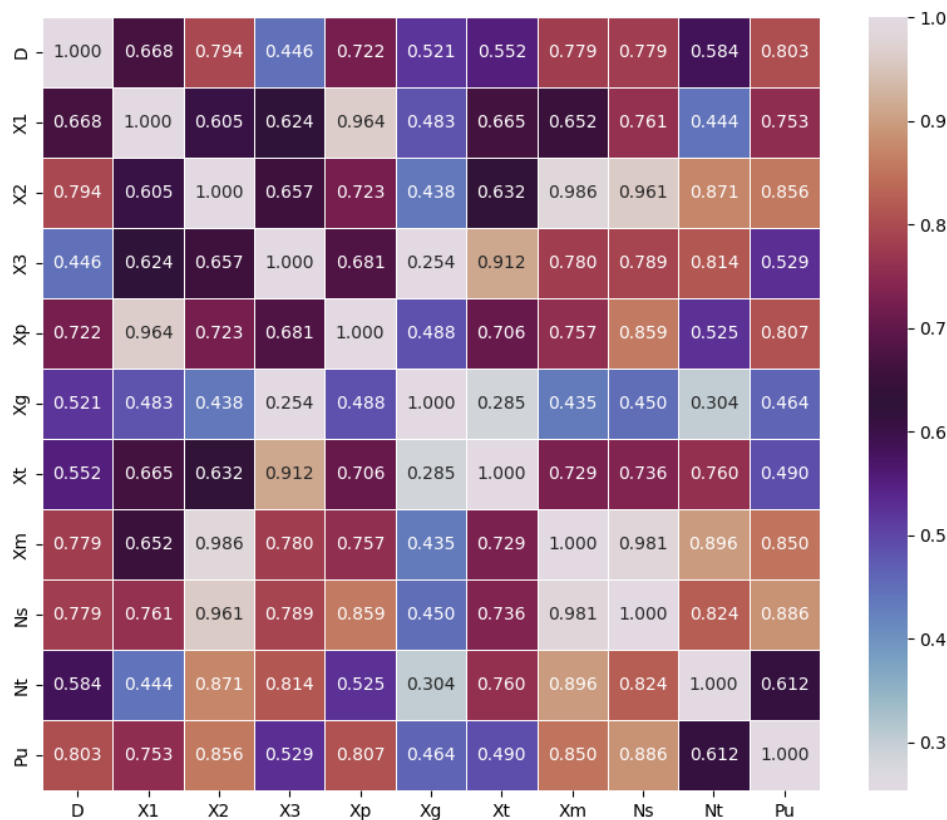


Figure 5. Presentation of the relationship of variables using the DC matrix.

The analysis of the distance correlation matrix revealed that the variables are significantly related to each other. Therefore, it is required to analyze the multicollinearity of each feature in estimating P_U. To analyze the feature multicollinearity, the variance inflation factor (VIF) has been utilized in this investigation. Khatti and Grover [45] introduced five different levels of feature multicollinearity, i.e., no (VIF = 0), weak (0 < VIF ≤ 2.5), considerable (2.5 < VIF ≤ 5.0), moderate (5.0 < VIF ≤ 10.0), and problematic (VIF > 10). The VIF (= 1/(1 - R²)) is determined using the determination coefficient (R²) obtained in regression analysis. It has been noted that (a) X_g feature has weak (=1.55) multicollinearity; (b) X_t feature has moderate (=5.66) multicollinearity; and (c) D (=10.47) and N_t (=293.77) show the problematic multicollinearity. Interestingly, the VIF values for X₁, X₂, X₃, X_p, X_m, and N_s have been obtained as infinite, indicating a problematic multicollinearity. Due to the problematic multicollinearity among the nine features, a sensitivity analysis was performed. The mathematical expression of cosine amplitude is as follows [46]:

$$CA = \frac{\sum_{i=1}^n X_i * Y_i}{\sqrt{\sum_{i=1}^n X_i^2 * \sum_{i=1}^n Y_i^2}} \tag{2}$$

where X_i and Y_i are the input(s) and target values. Figure 6 presents the sensitivity and contribution of each feature in predicting the bearing capacity of concrete piles. It can be observed that the N_s ($=0.9830 \approx 0.98$) is the most sensitivity feature in predicting P_U of reinforced concrete pile, followed by the X_2 ($=0.9809 \approx 0.98$), X_m ($=0.9732 \approx 0.97$), X_1 ($=0.9718 \approx 0.97$), D ($=0.9717 \approx 0.97$), N_t ($=0.9614 \approx 0.96$), X_g ($=0.9526 \approx 0.95$), and X_t ($=0.9092 \approx 0.91$). In addition, the N_s ($=10.6\%$), X_2 ($=10.57\%$), X_m ($=10.49\%$), X_1 ($=10.48\%$), D ($=10.48\%$), N_t ($=10.37\%$), X_g ($=10.27\%$), and X_t ($=9.8\%$) features have an excellent contribution in estimating the bearing capacity of the reinforced concrete piles. Therefore, the screened database can be utilized to develop the ABC_ANN, GA_ANN, GWO_ANN, HHO_ANN, and PSO_ANN models to predict the P_U of the reinforced concrete piles. The variables given in the screened database have been normalized using the min-max function ($y_{norm} = (x - x_{min}) / (x_{max} - x_{min})$); where x is the actual value, x_{min} and x_{max} are the minima and maximum of x array. In the previous studies, Ahmad et al., Liang et al., and Pham et al. utilized 80%, 70%, and 60% of the overall database to create the training database [47–49]. Therefore, 85% of the 194 datasets have been used to create a training database (164 datasets). The remaining 15% (30) of the datasets have been used to create the testing database.

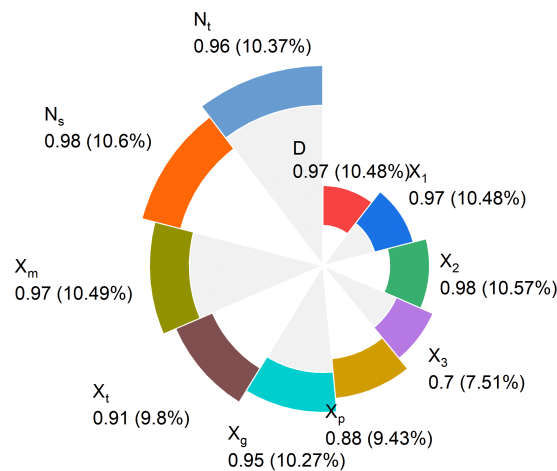


Figure 6. Presentation of sensitivity and contribution of each feature.

4. Results and Discussion

In this work, the ABC_ANN, GA_ANN, GWO_ANN, HHO_ANN, and PSO_ANN models have been developed to estimate the bearing capacity of reinforced concrete piles. To analyze the capabilities of each model, the RMSE, MAE, MAPE, NSE, VAF, R, and EVS metrics have been implemented. The reasons for implementing such metrics are: (a) RMSE is a good way to penalize big deviations since it highlights greater mistakes because of its squared component; (b) MAE is a robust measure of average error that is linear and simple to understand; (c) Scale-independent comparison is made possible by MAPE, which is particularly helpful when target values differ significantly; (d) NSE is widely used in environmental modeling and hydrology, measures the degree to which the predicted values correspond to the observed data; (e) VIF indicates the proportion of variability in the data that is captured by the model, serving as a measure of goodness-of-fit; (f) R metrics assess the degree of a linear connection between the observed and expected values; and (g) EVS measures the percentage of variation that the model can account for and provides information about its predictive ability. The combination of these measures offers a comprehensive and fair evaluation of the model’s forecast accuracy and dependability. The mathematical formulations of RMSE, MAE, MAPE, NSE, VAF, R, and EVS metrics are as follows:

$$RMSE = \sqrt{\frac{1}{n} \sum_{i=1}^n (A_i - P_i)^2} \tag{3}$$

$$MAE = \frac{1}{n} \sum_{i=1}^n |A_i - P_i| \tag{4}$$

$$MAPE = \frac{100}{n} \sum_{i=1}^n \left| \frac{A_i - P_i}{A_i} \right| \tag{5}$$

$$NSE = 1 - \frac{\sum_{i=1}^n (A_i - P_i)^2}{\sum_{i=1}^n (A_i - A_{mean})^2} \tag{6}$$

$$VAF = (1 - \frac{var(A_i - P_i)}{var(A_i)} * 100) \tag{7}$$

$$R = \frac{\sum_{i=1}^n (A_i - A_{mean})(P_i - P_{mean})}{\sqrt{\sum_{i=1}^n (A_i - A_{mean})^2} \cdot \sqrt{\sum_{i=1}^n (P_i - P_{mean})^2}} \tag{8}$$

$$EVS = 1 - \frac{var(A_i - P_i)}{var(A_i)} \tag{9}$$

where A_i is the actual P_U , P_i is the predicted P_U , A_{mean} is the mean of actual P_U , and P_{mean} is the mean of the predicted P_U . A soft computing model is considered optimal if it achieves RMSE = 0, MAE = 0, MAPE = 0, NSE = 1, VAF = 100, R = 1, and EVS = 1. Table 5 presents the summary of the performance of each model in the training (TRN) and testing (TST) phases.

Table 5. Summary of the model’s performance.

Models	Phase	RMSE	MAE	MAPE	NSE	VAF	R	EVS
ABC_ANN	TRN	54.897	36.229	3.690	0.9766	97.66	0.9882	0.98
	TST	108.008	83.424	7.427	0.8946	89.55	0.9535	0.90
GA_ANN	TRN	64.536	43.344	4.247	0.9676	96.76	0.9837	0.97
	TST	118.281	90.127	9.531	0.8736	88.18	0.9506	0.88
GWO_ANN	TRN	68.201	47.027	4.717	0.9639	96.39	0.9818	0.96
	TST	169.977	125.267	11.849	0.7390	75.81	0.9018	0.76
HHO_ANN	TRN	55.526	38.841	3.871	0.9760	97.60	0.9880	0.98
	TST	171.234	112.713	12.164	0.7352	73.74	0.8980	0.74
PSO_ANN	TRN	61.110	44.606	4.508	0.9710	97.10	0.9854	0.97
	TST	252.154	147.439	13.829	0.4257	42.94	0.7792	0.43

Note: Bold values present the optimal performance model.

4.1. Interpretation of Performance

In this work, the RMSE, MAE, MAPE, NSE, VAF, R, and EVS metrics have been analyzed to evaluate the capabilities of ABC_ANN, GA_ANN, GWO_ANN, HHO_ANN, and PSO_ANN models in estimating the bearing capacity of reinforced concrete piles, as reported in Table 3. The comparison reveals that each model has achieved an accuracy of over 98% in the training phase. Still, the PSO_ANN model has predicted the P_U with the least accuracy of 77.92% in the TST phase because of premature convergence and tuning of inertia weights and acceleration. The ABC_ANN model has gained the highest accuracy in both phases (TRN = 98.82% and TST = 95.35%). It has also been observed that the ABC_ANN model has predicted the P_U with the least residuals in the TRN (RMSE = 54.897 kN, MAE = 36.229 kN, MAPE = 3.690 kN) and TST (RMSE = 108.008 kN, MAE = 83.424 kN, MAPE = 7.427). Moreover, the NSE (TRN = 0.9766, TST = 0.8946), VAF (TRN = 97.66, TST = 89.55), and EVS (TRN = 0.98, TST = 0.90) metrics have demonstrated the precision of the ABC_ANN model in estimating the P_U .

Conversely, it has been found that the GA_ANN model has secured second place in estimating the P_U with an RMSE of 118.281kN, MAE of 90.127, MAPE of 9.531, NSE of 0.8736, VAF of 88.18, R of 0.9506, and EVS of 0.88 in the testing phase, comparatively higher than the GWO_ANN and HHO_ANN models. The fundamental study of the GWO algorithm reveals that the GWO_ANN model has achieved less performance due to high-dimensionality and loss of diversity. On the other hand, the HHO_ANN model has performed poorly due to its slow convergence and the imbalance between exploration and exploitation. Still, the HHO_ANN model has performed well (RMSE = 55.526kN, MAE = 38.841kN, MAPE = 3.871, NSE = 0.9760, VAF = 97.60, R = 0.9880, and EVS = 0.98) in the TRN phase. Figure 7 demonstrates the regression relationship between actual and predicted P_U using the optimized ANN models. Figure 7a shows a good agreement between actual and predicted P_U using the ABC_ANN model.

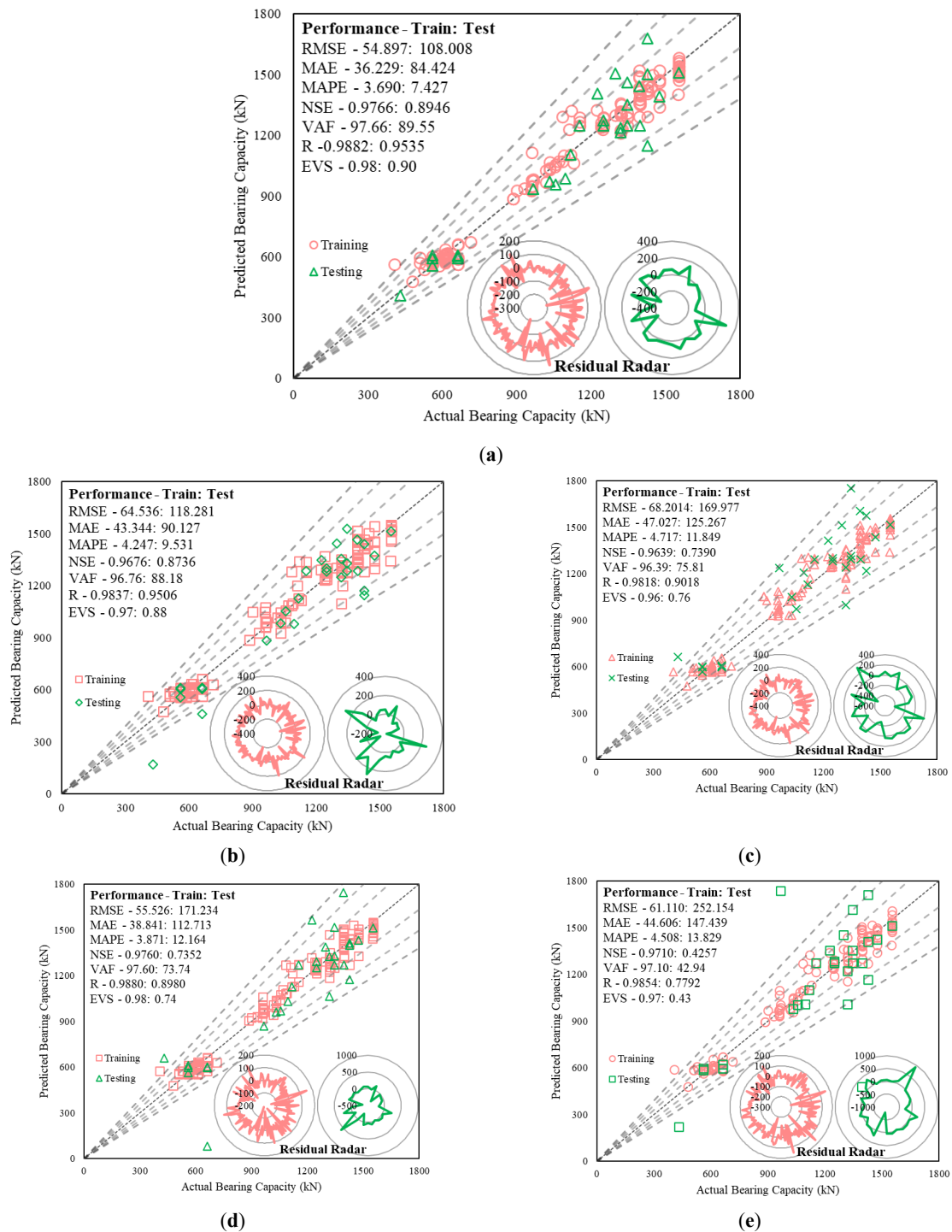


Figure 7. Depiction of the relationship between actual and predicted P_U using (a) ABC_ANN; (b) GA_ANN; (c) GWO_ANN; (d) HHO_ANN; and (e) PSO_ANN models.

4.2. Visual Interpretation of Models

4.2.1. Taylor Plot

A Taylor plot compares the correlation, standard deviation, and centered root mean square error (RMSE) of several models in relation to observed data, providing a graphical tool for evaluating the performance of numerous models at once. The radial distance, the angle, and the distance from the reference point, typically the observed data, indicate the standard deviation, correlation coefficient, and centered RMSE, respectively, for each model displayed as a point in a single polar plot. Models are directly compared due to this clear and simple display, which makes it simple to choose those that most closely resemble the statistical properties of the observed data. It is thought that models that are placed close to the reference location are more accurate and trustworthy. Figure 8

presents the comparison of accuracy and trustworthiness of the ABC_ANN, GA_ANN, GWO_ANN, HHO_ANN, and PSO_ANN models.

Figure 8a shows that the ABC_ANN, GA_ANN, GWO_ANN, HHO_ANN, and PSO_ANN models have estimated the P_U of the reinforced piles with the standard deviation of 355.55, 353.71, 355.44, 355.47, and 353.83kN, respectively, in the TRN phase, close to the standard deviation of the actual database, i.e., 359.87 kN. Moreover, the ABC_ANN, GA_ANN, GWO_ANN, HHO_ANN, and PSO_ANN models have estimated the P_U with the standard deviation of 362.31, 371.67, 384.68, 392.83, and 406.37 kN, respectively, in the TST phase, close to the standard deviation of the actual testing database, i.e., 338.42kN, as depicted in Figure 8b. The Taylor plots have also demonstrated the high prediction capabilities of the ABC_ANN model over the GA_ANN, GWO_ANN, HHO_ANN, and PSO_ANN models in estimating the bearing capacity of concrete piles.

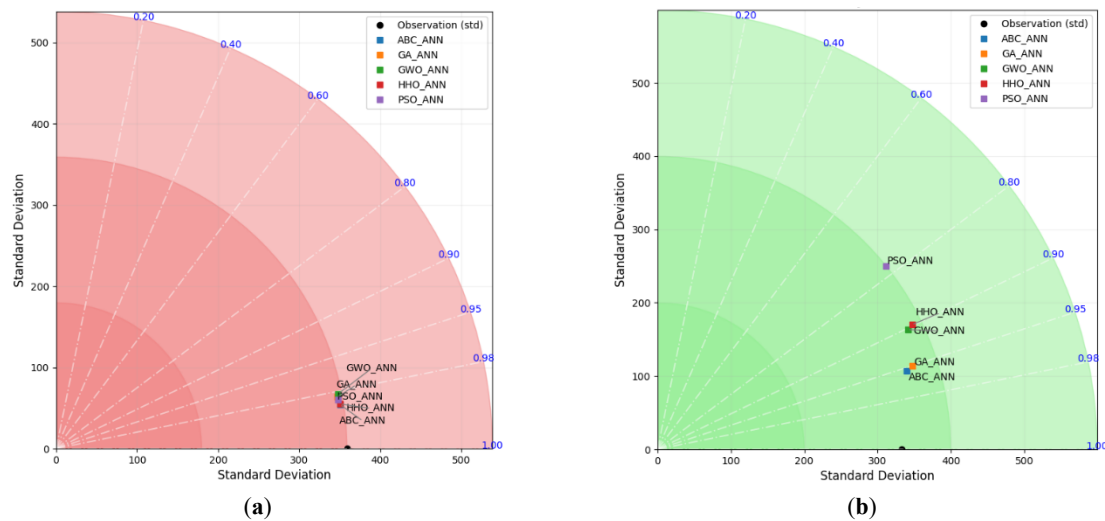


Figure 8. Illustration of the accuracy and trustworthiness of models using the Taylor plot in (a) training and (b) testing phase.

4.2.2. Score Analysis

The score analysis is the simplest statistical method to identify the optimal performance model. In this analysis, each performance metric is ranked in relation to the available models, i.e., $N = 5$, in this study. The model with performance close to the ideal values achieves a higher score for each metric. Thus, each model is ranked in each training and testing phase. The total score is calculated by summing the rank of each metric. The overall score for each model is calculated by summing the total ranks in the TRN and TST phases. Table 6 demonstrates that the ABC_ANN model has predicted the bearing capacity of concrete piles with an overall score of 70 (TRN + TST = 35 + 35), followed by GA_ANN (=44) and HHO_ANN (=43).

Table 6. Results of score analysis.

Models	Phase	RMSE	MAE	MAPE	NSE	VAF	R	EVS	Total	Overall
ABC_ANN	TRN	5	5	5	5	5	5	5	35	70
	TST	5	5	5	5	5	5	5	35	
GA_ANN	TRN	2	3	3	2	2	2	2	16	44
	TST	4	4	4	4	4	4	4	28	
GWO_ANN	TRN	1	1	1	1	1	1	1	7	27
	TST	3	2	3	3	3	3	3	20	
HHO_ANN	TRN	4	4	4	4	4	4	4	28	43
	TST	2	3	2	2	2	2	2	15	
PSO_ANN	TRN	3	2	2	3	3	3	3	19	26
	TST	1	1	1	1	1	1	1	7	

Note: Bold values present the optimal performance model.

4.2.3. REC Curve

The REC curve is a generalized graphical representation of the area under the curve (AUC) of the Receiver Operating Characteristics (ROC) curve, which is implemented in classification problems. The REC curve is drawn between error tolerance (X-axis) and accuracy (Y-axis). The maximum allowable absolute difference between the actual and predicted values is called the error tolerance. The accuracy is defined as the percentage of data points

for which the prediction falls within the specified error tolerance. The REC curve estimates the area over the curve (AOC = 1 – AUC), presenting a biased estimate of the model’s expected error. The REC curve defines an optimal performance model if it has the lowest AOC in both the training and testing phases. Figure 9a,b demonstrates that the ABC_ANN model has estimated the bearing capacity of concrete pile with the least AOC in TRN (=0.1982) and TST (=0.1078) phase, followed by the GA_ANN model.

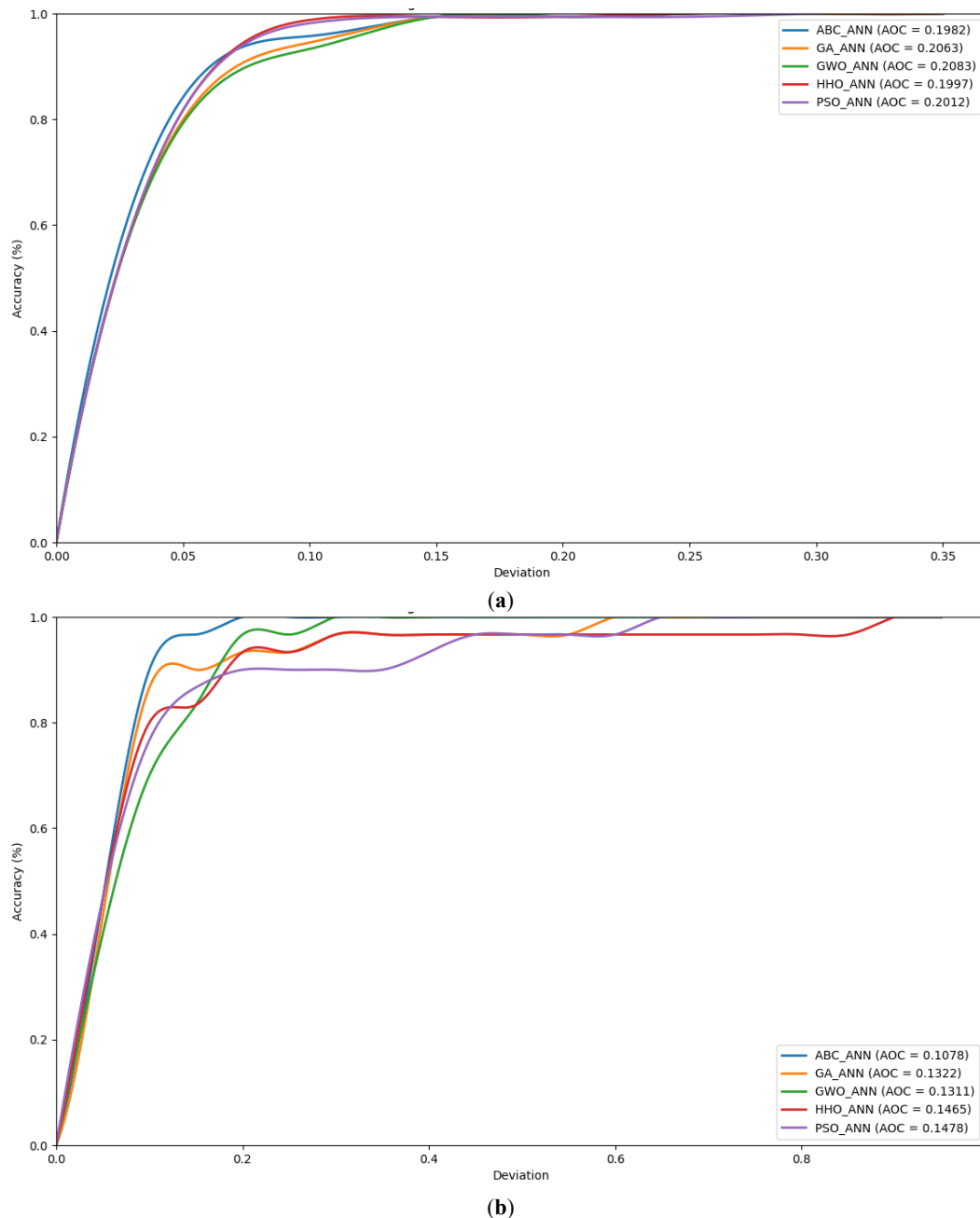


Figure 9. Illustration of REC curve in (a) training and (b) testing phase.

4.3. Generalizability Analysis

The performance comparison, Taylor plot, and REC curve have demonstrated that the ABC_ANN model has predicted P_U with excellent ability. Still, it is required to analyze the generalizability of each model in predicting the bearing capacity of concrete piles. To solve this issue, the generalizability, called external validation, of each model has been calculated and analyzed using the following equations [50]:

$$k = \frac{\sum_{i=0}^n (A_i \times P_i)}{\sum_{i=0}^n P_i^2} \tag{10}$$

$$k' = \frac{\sum_{i=0}^n (A_i \times P_i)}{\sum_{i=0}^n A_i^2} \tag{11}$$

$$R_o^2 = 1 - \frac{\sum_{i=1}^n P_i^2 (1 - k)^2}{\sum_{i=1}^n (P_i - P_{mean})} \tag{12}$$

$$R_o'^2 = 1 - \frac{\sum_{i=1}^n A_i^2 (1 - k')^2}{\sum_{i=1}^n (A_i - A_{mean})} \tag{13}$$

$$R_m = R^2 \times \left(1 - \sqrt{|R^2 - R_o^2|} \right) \tag{14}$$

$$|m| = \frac{R^2 - R_o^2}{R^2} \tag{15}$$

$$|n| = \frac{R^2 - R_o'^2}{R^2} \tag{16}$$

where k is the slope of the predicted vs actual values, k' is the slope of the actual vs predicted values, R_o^2 and $R_o'^2$ denotes the coefficients of determination of the predicted versus actual values and actual versus predicted values. $|m|$ and $|n|$ represent the factors for estimating the predictive power of the proposed models. The ideal values for these factors are (a) 0.85 to 1.15 for k and k' ; (b) close to 1 for R_o^2 , and $R_o'^2$; and (c) greater than 0.5 for R_m and (d) less than 0.1 for $|m|$ and $|n|$.

Table 7 presents the results of the generalizability analysis for each model in the training and testing phases. Table 7 demonstrates that the ABC_ANN model has predicted P_U with a good generalizability in training ($k = 1.000$, $k' = 0.998$, $R_o^2 = 1.000$, $R_o'^2 = 1.000$, $R_m = 0.827$, $|m| = 0.024$, and $|n| = 0.024$) and testing ($k = 0.998$, $k' = 0.994$, $R_o^2 = 1.000$, $R_o'^2 = 1.000$, $R_m = 0.635$, $|m| = 0.100$, and $|n| = 0.099$) phase, comparatively better than the GA_ANN, GWO_ANN, HHO_ANN, and PSO_ANN models.

Table 7. Summary of generalizability analysis.

Models	Phase	k	k'	R_o^2	$R_o'^2$	R_m	$ m $	$ n $
ABC_ANN	TRN	1.000	0.998	1.000	1.000	0.827	0.024	0.024
	TST	0.998	0.994	1.000	1.000	0.635	0.100	0.099
GA_ANN	TRN	1.000	0.997	1.000	1.000	0.794	0.033	0.033
	TST	1.011	0.979	0.999	0.995	0.625	0.105	0.101
GWO_ANN	TRN	1.000	0.996	1.000	1.000	0.781	0.037	0.037
	TST	0.943	1.040	0.967	0.981	0.494	0.190	0.206
HHO_ANN	TRN	1.000	0.998	1.000	1.000	0.825	0.025	0.024
	TST	0.987	0.990	0.999	0.999	0.453	0.238	0.239
PSO_ANN	TRN	0.999	0.998	1.000	1.000	0.806	0.030	0.030
	TST	0.974	0.978	0.994	0.994	0.229	0.638	0.637

Note: Bold values present the optimal performance model.

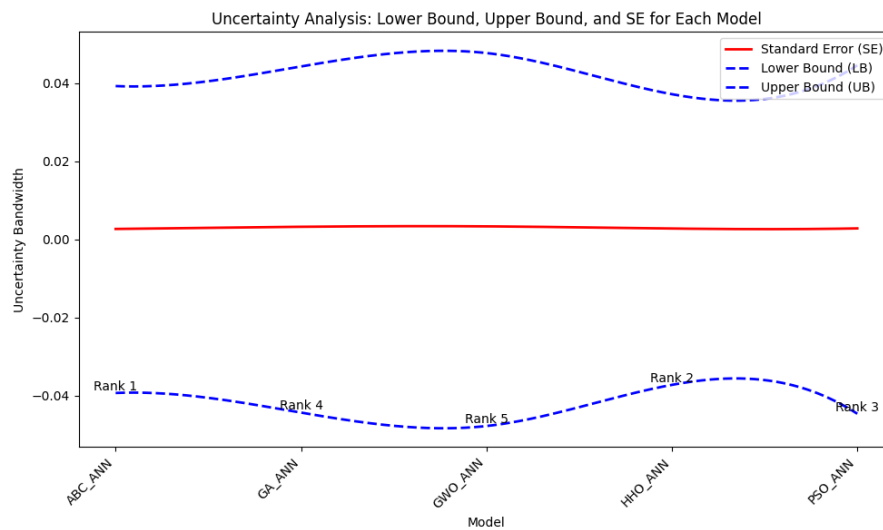
4.4. Uncertainty Analysis

The uncertainty analysis is a method for checking the accuracy and reliability of soft computing models in regression problems. This analysis computes confidence parameters (e.g., upper bound-UB, lower bound-LB, and the width of confidence bound-WCB), margin of error at 95% confidence level (ME), standard deviation (SD), mean of error (MOE), and standard error (SE) for the predicted values of each soft computing model. The WCB is a difference between UB and LB. Each soft computing model is ranked based on the least values of UB, LB, WCB, ME, SD, MOE, and SE. The model ranks first and is recognized as a highly accurate and reliable soft computing model. Table 8 summarizes the results of the uncertainty analysis, and Figure 10 presents the comparison of the uncertainty bandwidth with ranks. It can be observed that the ABC_ANN model has achieved the first rank in both phases in predicting P_U . Conversely, the PSO_ANN model has achieved the fifth rank in the testing phase, presenting poor robustness.

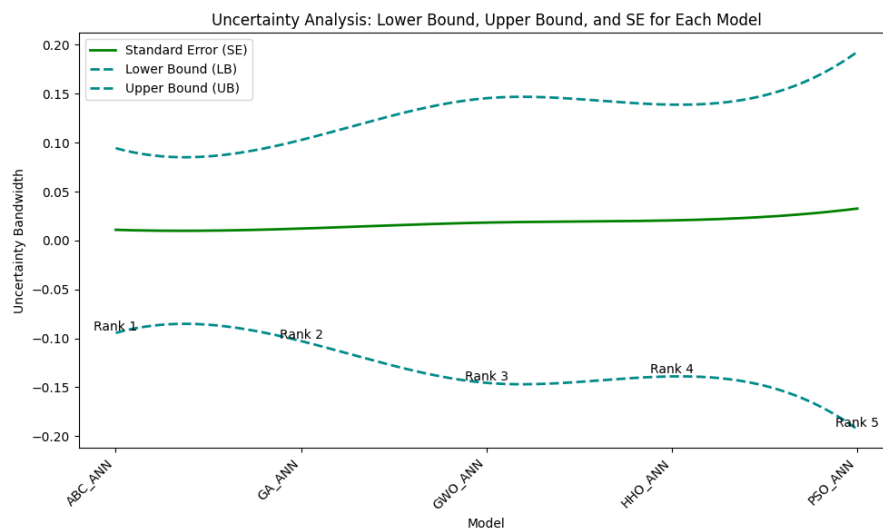
Table 8. Summary of uncertainty analysis results.

Model	MOE	SD	SE	ME	LB	UB	WCB
<i>Training Phase</i>							
ABC_ANN	0.034	0.035	0.003	0.005	0.039	0.039	0.005
GA_ANN	0.038	0.042	0.003	0.006	0.044	0.044	0.006
GWO_ANN	0.041	0.043	0.003	0.007	0.048	0.048	0.007
HHO_ANN	0.032	0.036	0.003	0.006	0.037	0.037	0.006
PSO_ANN	0.039	0.037	0.003	0.006	0.045	0.045	0.006
<i>Testing Phase</i>							
ABC_ANN	0.073	0.060	0.011	0.021	0.094	0.094	0.021
GA_ANN	0.079	0.067	0.012	0.024	0.103	0.103	0.024
GWO_ANN	0.110	0.100	0.018	0.036	0.145	0.145	0.036
HHO_ANN	0.099	0.113	0.021	0.040	0.139	0.139	0.040
PSO_ANN	0.129	0.179	0.033	0.064	0.193	0.193	0.064

Note: Bold values present the optimal performance model.



(a)



(b)

Figure 10. Illustration of uncertainty bandwidth in (a) training and (b) testing phase.

4.5. Discussion on Results

The performance metrics [51,52], Taylor plot, score analysis, REC curve, generalizability, and uncertainty analyses have demonstrated that the ABC_ANN model has outperformed the GA_ANN, GWO_ANN, HHO_ANN, and PSO_ANN models in estimating the bearing capacity of concrete piles. Still, it is required to understand the behaviour of each model in predicting the bearing capacity of concrete piles for an unseen database. Therefore, the curve fitting analysis has been performed. A soft computing model shows under, over, and best fit

behaviour in the regression process [53]. This investigation computes the overfitting by computing the test-to-train RMSE ratio. Figure 11 compares the overfitting of each model. It is noteworthy that the ABC_ANN model has predicted the bearing capacity of concrete piles with the least overfitting, i.e., 1.97, demonstrating high efficiency on the unseen database, followed by the HHO_ANN model. It can be seen that the GWO_ANN model has achieved an overfitting of 3.70 in this investigation because GWO's strong exploitation and fast convergence fit the training data (including noise) too precisely. In addition, the feature multicollinearity analysis has demonstrated that (a) X_g feature has weak (=1.55) multicollinearity; (b) X_t feature has moderate (=5.66) multicollinearity; and (c) D (=10.47) and N_t (=293.77) show the problematic multicollinearity. Conversely, the X_1 , X_2 , X_3 , X_p , X_m , and N_s features have problematic multicollinearity. Therefore, the ABC_ANN model has obtained an overfitting of 1.97, comparatively less than other ANN models.

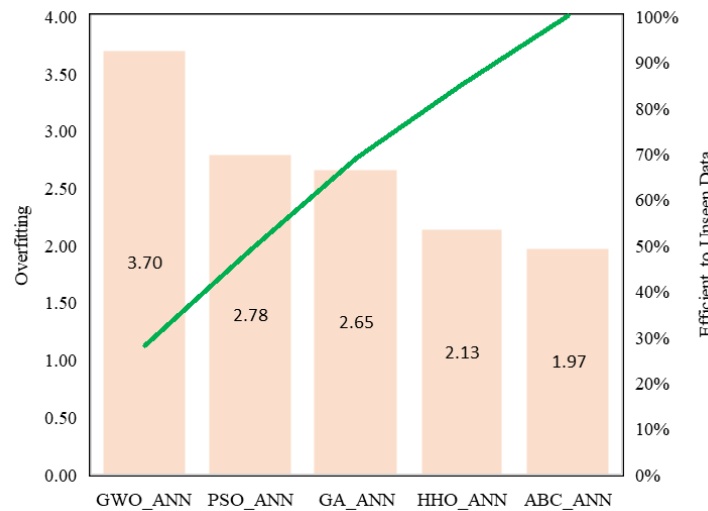


Figure 11. Depiction of the comparison of the overfitting of each model.

The discrete metrics, i.e., prediction of change in direction (PCD) and a-indices (a_{10} , a_{20} , and a_{30}), have been implemented to measure the accuracy of each model in both phases, using the following Equations (17)–(20) and (53). Figure 12 presents the visual comparison of discrete accuracy metrics in the training and testing phases.

$$PCD = \frac{1}{n-1} \sum_{i=2}^n I((P_i - P_{i-1})(A_i - A_{i-1}) > 0) \tag{13}$$

$$a_{10} = \frac{1}{n} \sum_{i=1}^n \begin{cases} 1, & \text{if } |P_i - A_i|/A_i \leq 0.1 \\ 0, & \text{Otherwise} \end{cases} \tag{14}$$

$$a_{20} = \frac{1}{n} \sum_{i=1}^n \begin{cases} 1, & \text{if } |P_i - A_i|/A_i \leq 0.2 \\ 0, & \text{Otherwise} \end{cases} \tag{15}$$

$$a_{30} = \frac{1}{n} \sum_{i=1}^n \begin{cases} 1, & \text{if } |P_i - A_i|/A_i \leq 0.3 \\ 0, & \text{Otherwise} \end{cases} \tag{16}$$

Figure 12 shows that the ABC_ANN model has estimated the bearing capacity with higher PCD, a-index in training (PCD = 0.90, a_{10} = 0.92, a_{20} = 0.99, and a_{30} = 0.99) and testing (PCD = 0.79, a_{10} = 0.80, a_{20} = 1.00, and a_{30} = 1.00) phase, close to the ideal values, i.e., 1. In addition, it can be observed that the GWO_ANN model has predicted the bearing capacity of concrete pile with the least accuracies in training (PCD = 0.88, a_{10} = 0.88, a_{20} = 0.99, and a_{30} = 0.99) and testing (PCD = 0.76, a_{10} = 0.67, a_{20} = 0.80, and a_{30} = 0.90) phase. The overfitting analysis and discrete metrics have demonstrated that the ABC_ANN model is an optimal performance model to estimate the bearing capacity of concrete piles. To analyze the robustness of the ABC_ANN model, a comparison between the ABC_ANN and published models has been drawn, as shown in Table 9. It can be observed that the ABC_ANN model has also outperformed the published models and showed its robustness in estimating the bearing capacity of concrete piles.

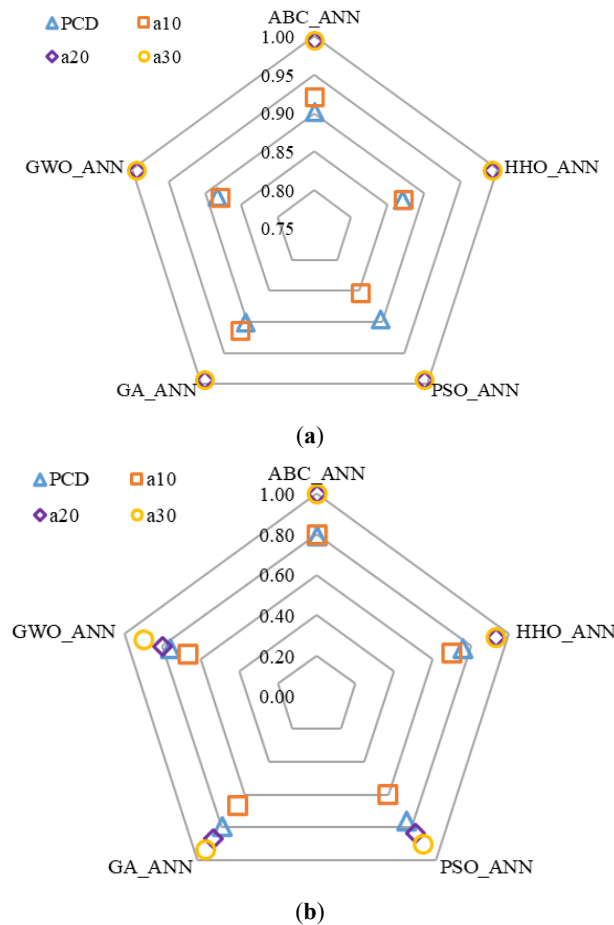


Figure 12. Illustration of comparison of discrete accuracy of models in (a) training and (b) testing phase.

Table 9. Comparison of the ABC_ANN and published models.

S. No.	References	Features: Data	Model	Test RMSE
1	Zhao [11]	c, ϕ , γ , ϕ' , F, A, L [231 × 7]	NB_CO	228.6274
2	Umar et al. [12]	A, L, SPT _n , D [125 × 4]	IGPR	278.4500
3	Sun et al. [14]	v, ϕ , E, S ₁ , L, S ₂ , S ₃ , S ₄ [60 × 8]	HGS_XGBoost	169.4300
4	Seo et al. [15]	d, L, D _H (EOID, Restrike), Ram, S (EOID, Restrike), T, D [217 × 9]	DNN	661.1890
5	Seo et al. [15]	d, L, D _H (EOID, Restrike), Ram, S (EOID, Restrike), T, D [217 × 9]	DNN	1142.4000
6	Hu [20]	c, ϕ , γ , ϕ' , F, A, L [231 × 7]	RSA_MLP	126.7000
7	Cai et al. [24]	c, ϕ , γ , ϕ' , F, A, L [231 × 7]	IGWO_GPR	276.1000
8	Yang et al. [27]	c, ϕ , γ , ϕ' , F, A, L [231 × 7]	PDO_LSSVM	213.7700
9	Khatti et al. [33]	d, L, qv, PI, Su, T, Qf [126 × 7]	GA_GRVM	146.3962
10	Present study	d, X₁, X₂, X₃, X_p, X_g, X_t, X_m, N_s, N_t [200 × 10]	ABC_ANN	108.0080

Note: Bold values demonstrate the optimal performance model.

5. Summary and Conclusions

This study evaluated the predictive performance of five hybrid ANN models optimized with Particle Swarm Optimization (PSO), Harris Hawks Optimization (HHO), Grey Wolf Optimization (GWO), Genetic Algorithm (GA), and Artificial Bee Colony (ABC) to estimate the bearing capacity of reinforced concrete piles in alluvial soils. A dataset of 194 samples, obtained from the literature, was preprocessed, with 164 and 30 data points used for training and testing, respectively. The models were systematically assessed using RMSE, MAE, MAPE, NSE, VAF, R, and EVS metrics, along with Taylor plots, score analysis, regression error characteristic curves, generalizability, and uncertainty analyses.

- Capabilities of Models:** Among the tested models, the ABC_ANN demonstrated superior predictive accuracy (RMSE = 108.01 kPa, MAE = 83.42 kPa, MAPE = 7.43%, R = 0.95, NSE = 0.89, VAF = 89.55%, EVS = 0.90), consistently outperforming PSO_ANN, HHO_ANN, GWO_ANN, and GA_ANN. Its robustness was further confirmed by Taylor plots, REC values, score (=35), and uncertainty analysis.

- **Optimal Performance Model**—The ABC_ANN model was identified as the optimal performance model, achieving the highest generalizability and the lowest prediction error in both training and testing phases.
- **Impact of Feature Multicollinearity**—Variance inflation factor (VIF) analysis revealed significant multicollinearity among features such as pile depth, soil layer depth, ground elevation, pile tip elevation, and standard penetration blow counts. This feature dependency caused mild overfitting (1.97) in the ABC_ANN model. Despite this, these features were shown to be essential contributors to accurate predictions.
- **Novelty of the Study:** This work is the first to comprehensively compare PSO-, HHO-, GWO-, GA-, and ABC-optimized ANN models for predicting the bearing capacity of reinforced concrete piles. It introduces the use of VIF-based multicollinearity analysis to quantify the influence of correlated geotechnical features on the performance and overfitting behavior of hybrid ANN models.

The findings establish the ABC_ANN model as a reliable and robust tool for geotechnical engineering applications. By providing accurate predictions without the need for extensive in-situ or laboratory testing, the model can reduce costs, minimize the reliance on heavy equipment, and support engineers and designers in foundation design and construction planning. This study was constrained by the use of a limited database, which represents its main limitation. Future studies should expand the dataset and explore other advanced soft computing methods such as Random Forest (RF), Kernel-based Extreme Learning Machine (KELM), XGBoost, Gated Recurrent Unit (GRU), and Convolutional Neural Networks (CNN) combined with metaheuristic optimization to further enhance prediction accuracy. In summary, this investigation introduces the ABC_ANN as an optimal hybrid model that combines predictive robustness with practical applicability, offering a valuable decision-support tool for geotechnical engineers in assessing the bearing capacity of piles in complex soil conditions.

Author Contributions

J.K.: Conceptualization, literature review, manuscript preparation, application of AI models, machine learning model development, methodological development, statistical analysis, detailing, editing, and overall analysis; D.-P.N.K.: Data compilation and analysis, manuscript preparation, detailing, and editing. All authors have read and agreed to the published version of the manuscript.

Funding

This research received no external funding.

Institutional Review Board Statement

Not applicable.

Informed Consent Statement

Not applicable.

Data Availability Statement

The details of the database are provided in the manuscript. The models and codes developed for this research are available from the corresponding author upon reasonable request.

Conflicts of Interest

The authors declare no conflict of interest. Given the role as Editorial Board Member, Jitendra Khatti had no involvement in the peer review of this paper and had no access to information regarding its peer-review process. Full responsibility for the editorial process of this paper was delegated to another editor of the journal.

Use of AI and AI-Assisted Technologies

No AI tools were utilized for this paper.

Reference

1. Coyle, H.M.; Sulaiman, I.H. Bearing capacity of foundation piles: State of the art. *Highw. Res. Rec.* **1970**, *333*, 87.
2. Wrana, B. Pile load capacity—calculation methods. *Stud. Geotech. Et Mech.* **2015**, *37*, 83–93.
3. Meyerhof, G.G. Some recent research on the bearing capacity of foundations. *Can. Geotech. J.* **1963**, *1*, 16–26. <https://doi.org/10.1139/t63-003>.

4. Jeong, S.; Kim, D.; Park, J. Empirical bearing capacity formula for steel pipe prebored and precast piles based on field tests. *Int. J. Geomech.* **2021**, *21*, 04021165. [https://doi.org/10.1061/\(ASCE\)GM.1943-5622.0002112](https://doi.org/10.1061/(ASCE)GM.1943-5622.0002112).
5. Alielahi, H.; Adampira, M. Comparison between empirical and experimental ultimate bearing capacity of bored piles—A case study. *Arab. J. Geosci.* **2016**, *9*, 78. <https://doi.org/10.1007/s12517-015-2211-y>.
6. Shatnawi A.; Bodour W.A.; Abdel-Jaber M.T.; et al. Empirical formulas to predict the axial capacity of driven piles using in-situ dynamic load testing data. *Int. J. Mach. Learn. Comput.* **2019**, *9*, 129–134. <https://doi.org/10.18178/ijmlc.2019.9.2.776>.
7. Ribeiro, D.B.; Pereira, J.L.J.; Lorena, A.C. Optimizing Empirical Methods for Calculating the Bearing Capacity of Concrete Piles. In *Encontro Nacional de Inteligência Artificial e Computacional (ENIAC)*; SBC: Belém, Brazil, 2024; pp. 132–143. <https://doi.org/10.5753/eniac.2024.245084>.
8. Eslami, A.; Aflaki, E.; Hosseini, B. Evaluating CPT and CPTu based pile bearing capacity estimation methods using Urmieh Lake Causeway piling records. *Sci. Iran.* **2011**, *18*, 1009–1019. <https://doi.org/10.1016/j.scient.2011.09.003>.
9. Mijena, E.H. A comparison of friction piles bearing capacity based on theoretical and empirical mathematical models. Master's Thesis, Norwegian University of Science and Technology, Trondheim, Norway, 2012.
10. Luo, Z.; Dong, F. Statistical investigation of bearing capacity of pile foundation based on Bayesian reliability theory. *Adv. Civ. Eng.* **2019**, *2019*, 9858617. <https://doi.org/10.1155/2019/9858617>.
11. Zhao, Z. A Reliable Prediction Method to Forecast Pile Bearing Capacity Using Classic NB Base Hybrid Schemes. *J. Inst. Eng. (India) Ser. A* **2025**, *106*, 31–44. <https://doi.org/10.1007/s40030-024-00852-y>.
12. Umar, I.H.; Salga, M.S.; Lin, H.; et al. Performance characterisation of machine learning models for geotechnical axial pile load capacity estimation: An enhanced GPR-based approach. *Geomech. Geoengin.* **2025**, *20*, 846–887. <https://doi.org/10.1080/17486025.2025.2468645>.
13. Suzuki, N.; Nagai, K. Updating pile bearing capacity estimation using multiple piling data and spatial correlation. *Georisk: Assess. Manag. Risk Eng. Syst. Geohazards* **2025**, *19*, 698–714. <https://doi.org/10.1080/17499518.2024.2449377>.
14. Sun, Z.-J.; Han, Y.-F.; Jiang, F.; et al. Prediction of ultimate bearing capacity of single pile in composite formation based on HGS-XGBoost algorithm. *Appl. Geophys.* **2025**, 1–18. <https://doi.org/10.1007/s11770-025-1203-2>.
15. Sun, Z.; Han, Y.; Jiang, F.; et al. Leveraging data-driven machine learning techniques to enhance bearing capacity estimation in prebored and precast piles. *Expert Syst. Appl.* **2025**, *285*, 128070. <https://doi.org/10.1016/j.eswa.2025.128070>.
16. Onyelowe, K.C.; Hanandeh, S.; Kamchoom, V.; et al. Developing advanced datadriven framework to predict the bearing capacity of piles on rock. *Sci. Rep.* **2025**, *15*, 11051. <https://doi.org/10.1038/s41598-025-96186-1>.
17. Nhat, L.V.; Anh, T.N.; Van, H.T.V. Ultimate bearing capacity of bored piles in clayey sand determined using artificial neural networks. *Transp. Infrastruct. Geotechnol.* **2025**, *12*, 132. <https://doi.org/10.1007/s40515-025-00592-x>.
18. Khan, A.; Khan, M.; Khan, W.A.; et al. Predicting pile bearing capacity using gene expression programming with SHapley Additive exPlanation interpretation. *Discov. Civ. Eng.* **2025**, *2*, 58. <https://doi.org/10.1007/s44290-025-00215-x>.
19. Ji, Y. Estimation of pile-bearing capacity of rocks via reliable hybridization techniques. Multiscale and Multidisciplinary Modeling. *Exp. Des.* **2025**, *8*, 103. <https://doi.org/10.1007/s41939-024-00674-2>.
20. Hu, J.; Xia, C.; Wu, J.; et al. Estimating the pile-bearing capacity utilizing a reliable machine-learning approach. *Multiscale Multidiscip. Model. Exp. Des.* **2025**, *8*, 1–32. <https://doi.org/10.1007/s41939-025-00761-y>.
21. Fattahi, H.; Ghaedi, H. Forecasting Pile Bearing Capacity Using an Innovative RES-Based Approach. *Indian Geotech. J.* **2025**, *55*, 1629–1642. <https://doi.org/10.1007/s40098-024-01036-y>.
22. Eslami, A.; Rahimi, A.; Nobahar, M. Ultimate load bearing of helical piles prediction and evaluation using machine learning-based algorithms. *Geomech. Geoengin.* **2025**, *20*, 661–686. <https://doi.org/10.1080/17486025.2024.2438077>.
23. Chen, B.; Hai, M.; Di, G.; et al. Enhanced Dung Beetle Optimizer-Optimized KELM for Pile Bearing Capacity Prediction. *Build.* **2025**, *15*, 2654. <https://doi.org/10.3390/buildings15152654>.
24. Cai, L.; Zhu, D.; Xu, K. The implementation of a machine-learning-based model utilizing meta-heuristic algorithms for predicting pile bearing capacity. *Indian Geotech. J.* **2025**, *55*, 210–225. <https://doi.org/10.1007/s40098-024-00933-6>.
25. Yousheng, D.; Keqin, Z.; Zhongju, F.; et al. Machine learning based prediction model for the pile bearing capacity of saline soils in cold regions. In *Structures*; Elsevier: Amsterdam, The Netherlands, 2024. <https://doi.org/10.1016/j.istruc.2023.105735>.
26. Yaychi, B.M.; Esmacili-Falak, M. Estimating axial bearing capacity of driven piles using tuned random forest frameworks. *Geotech. Geol. Eng.* **2024**, *42*, 7813–7834. <https://doi.org/10.1007/s10706-024-02952-9>.
27. Yang, X. Prediction of pile-bearing capacity using Least Square Support Vector Regression: Individual and hybrid models development. *Multiscale Multidiscip. Model. Exp. Des.* **2024**, *7*, 2701–2715. <https://doi.org/10.1007/s41939-023-00357-4>.
28. Xu, M.; Zhu, Z. Utilizing meta-heuristic algorithms for load-bearing capacity prediction in piles with support vector regression. *Multiscale Multidiscip. Model. Exp. Des.* **2024**, *7*, 5445–5459. <https://doi.org/10.1007/s41939-024-00527-y>.
29. Tran, T.H.; Nguyen, B.P.; Tran, T.D. Machine learning applications in Pile load capacity prediction: Advanced analysis of pile driving forces and depths in urban Ho Chi Minh City construction sites. *Indian Geotech. J.* **2024**, *55*, 1795–1800. <https://doi.org/10.1007/s40098-024-01055-9>.

30. Shen, Y. Optimized systems of multi-layer perceptron predictive model for estimating pile-bearing capacity. *J. Eng. Appl. Sci.* **2024**, *71*, 52. <https://doi.org/10.1186/s44147-024-00386-x>.
31. Arbi, S.J.; Hassan, W.; Khalid, U.; et al. Optimized machine learning-based enhanced modeling of pile bearing capacity in layered soils using random and grid search techniques. *Earth Sci. Inform.* **2025**, *18*, 1–21. <https://doi.org/10.1007/s12145-025-01784-2>.
32. Kumar, M.; Kumar, D.R.; Khatti, J.; et al. Prediction of bearing capacity of pile foundation using deep learning approaches. *Front. Struct. Civ. Eng.* **2024**, *18*, 870–886. <https://doi.org/10.1007/s11709-024-1085-z>.
33. Khatti, J.; Khanmohammadi, M.; Fissaha, Y. Prediction of time-dependent bearing capacity of concrete pile in cohesive soil using optimized relevance vector machine and long short-term memory models. *Sci. Rep.* **2024**, *14*, 32047. <https://doi.org/10.1038/s41598-024-83784-8>.
34. Karakaş, S.; Taşkın, G.; Ülker, M.B.C. Re-evaluation of machine learning models for predicting ultimate bearing capacity of piles through SHAP and Joint Shapley methods. *Neural Comput. Appl.* **2024**, *36*, 697–715. <https://doi.org/10.1007/s00521-023-09053-3>.
35. Gu, W.; Liao, J.; Cheng, S. Bearing capacity prediction of the concrete pile using tunned ANFIS system. *J. Eng. Appl. Sci.* **2024**, *71*, 39. <https://doi.org/10.1186/s44147-024-00369-y>.
36. Gang, L. Improving the estimation of the pile bearing capacity via hybridization technique based on adaptive network based fuzzy inference. *J. Ambient. Intell. Humaniz. Comput.* **2024**, *15*, 4043–4060. <https://doi.org/10.1007/s12652-024-04878-9>.
37. Amjad, M.; Ahmad, I.; Ahmad, M.; et al. Prediction of pile bearing capacity using XGBoost algorithm: Modeling and performance evaluation. *Appl. Sci.* **2022**, *12*, 2126. <https://doi.org/10.3390/app12042126>.
38. Karaboga, D. An idea based on honey bee swarm for numerical optimization. *Dep. Comput. Sci.* **2005**, 1–10.
39. Mirjalili, S.; Mirjalili, S.M.; Lewis, A. Grey wolf optimizer. *Adv. Eng. Softw.* **2014**, *69*, 46–61. <https://doi.org/10.1016/j.advengsoft.2013.12.007>.
40. Heidari, A.A.; Mirjalili, S.; Faris, H.; et al. Harris hawks optimization: Algorithm and applications. *Future Gener. Comput. Syst.* **2019**, *97*, 849–872. <https://doi.org/10.1016/j.future.2019.02.028>.
41. Kennedy, J.; Eberhart, R. Particle swarm optimization. In Proceedings of ICNN'95-International Conference on Neural Networks, Perth, WA, Australia, 27 November–1 December 1995; Volume 4. <https://doi.org/10.1109/ICNN.1995.488968>.
42. Edelman, D.; Móri, T.F.; Székely, G.J. On relationships between the Pearson and the distance correlation coefficients. *Stat. Probab. Lett.* **2021**, *169*, 108960. <https://doi.org/10.1016/j.spl.2020.108960>.
43. Smith, G.N. Probability and statistics in civil engineering. In *Collins Professional and Technical Books*; Nichols Publishing Company: New York, NY, USA, 1986; p. 244.
44. Hair, J.F.; Wolfinbarger, M.; Money, A.H.; et al. *Essentials of Marketing Research*, 3rd ed.; McGraw-Hill/Irwin: New York, NY, USA, 2013.
45. Khatti, J.; Grover, K.S. Prediction of compaction parameters for fine-grained soil: Critical comparison of the deep learning and standalone models. *J. Rock Mech. Geotech. Eng.* **2023**, *15*, 3010–3038. <https://doi.org/10.1016/j.jrmge.2022.12.034>.
46. Asteris, P.G.; Skentou, A.D.; Bardhan, A.; et al. Predicting concrete compressive strength using hybrid ensembling of surrogate machine learning models. *Cem. Concr. Res.* **2021**, *145*, 106449. <https://doi.org/10.1016/j.cemconres.2021.106449>.
47. Ahmad, M.; Hu, J.L.; Ahmad, F.; et al. Supervised learning methods for modeling concrete compressive strength prediction at high temperature. *Mater.* **2021**, *14*, 1983. <https://doi.org/10.3390/ma14081983>.
48. Liang, W.; Luo, S.; Zhao, G.; et al. Predicting hard rock pillar stability using GBDT, XGBoost, and LightGBM algorithms. *Math.* **2020**, *8*, 765. <https://doi.org/10.3390/math8050765>.
49. Pham, T.A.; Tran, V.Q.; Vu, H.L.T.; et al. Design deep neural network architecture using a genetic algorithm for estimation of pile bearing capacity. *PLoS ONE* **2020**, *15*, e0243030. <https://doi.org/10.1371/journal.pone.0243030>.
50. Golbraikh, A.; Tropsha, A. Beware of q²! *J. Mol. Graph. Model.* **2002**, *20*, 269–276. [https://doi.org/10.1016/S1093-3263\(01\)00123-1](https://doi.org/10.1016/S1093-3263(01)00123-1).
51. Huang, J.; Asteris, P.G.; Manafi Khajeh Pasha, S.; et al. A new auto-tuning model for predicting the rock fragmentation: A cat swarm optimization algorithm. *Eng. Comput.* **2022**, *38*, 2209–2220. <https://doi.org/10.1007/s00366-020-01207-4>.
52. Mohammed, A.; Kurda, R.; Armaghani, D.J.; et al. Prediction of compressive strength of concrete modified with fly ash: Applications of neuro-swarm and neuro-imperialism models. *Adv. Concr. Constr.* **2021**, *11*, 489–512. <https://doi.org/10.12989/acc.2021.11.5.489>.
53. Mawlood, Y.; Salih, A.; Hummadi, R.; et al. Comparison of artificial neural network (ANN) and linear regression modeling with residual errors to predict the unconfined compressive strength and compression index for Erbil City soils, Kurdistan-Iraq. *Arab. J. Geosci.* **2021**, *14*, 485. <https://doi.org/10.1007/s12517-021-06712-4>.